

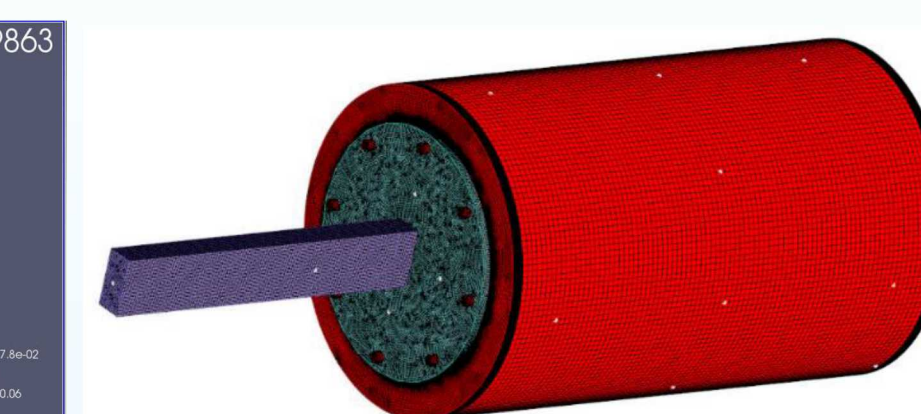
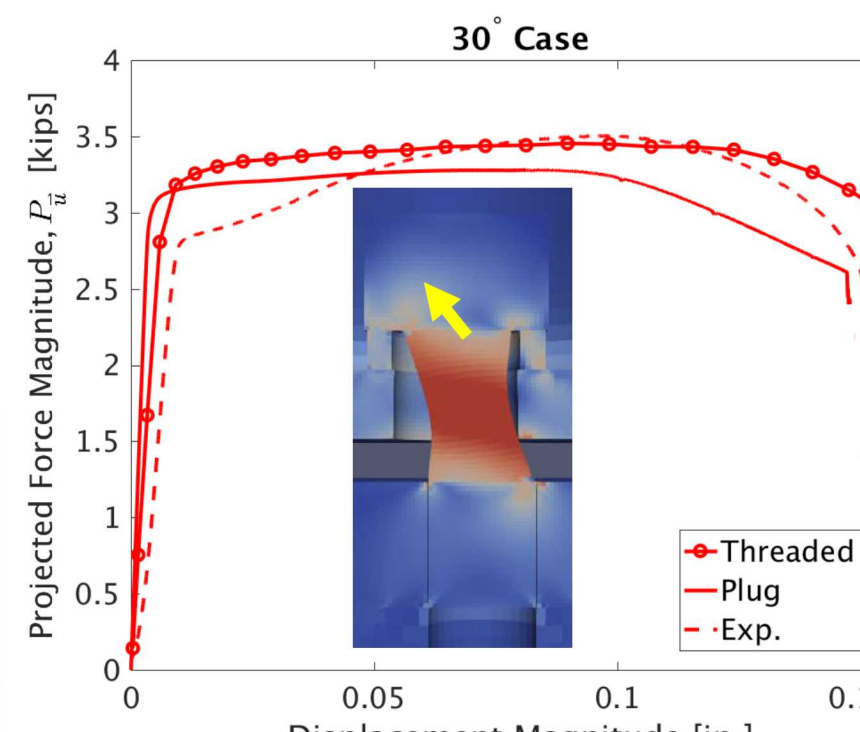
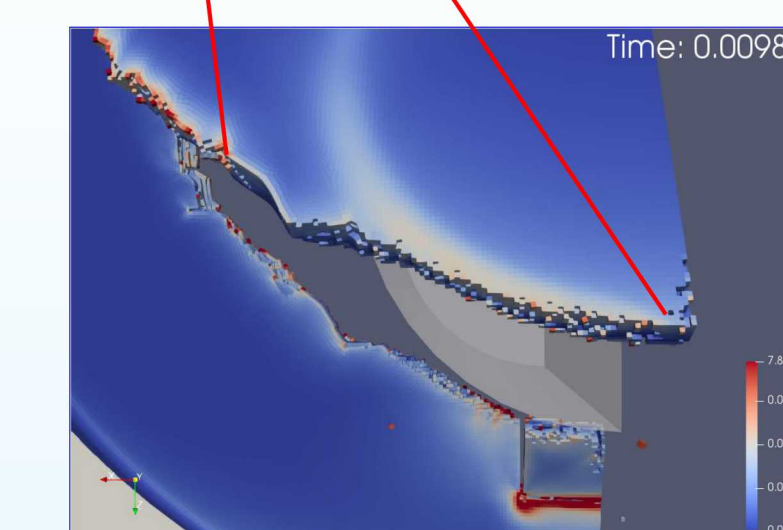
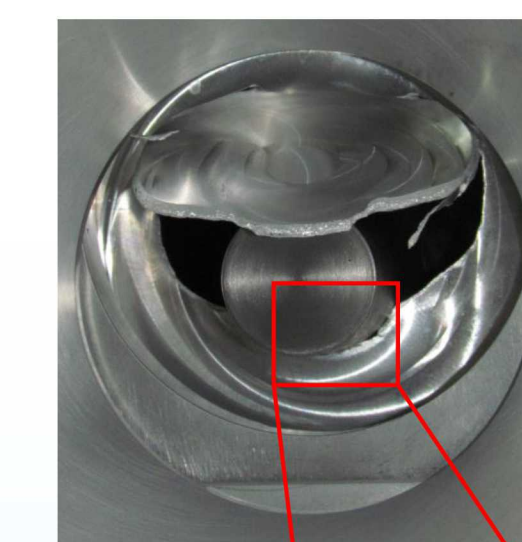
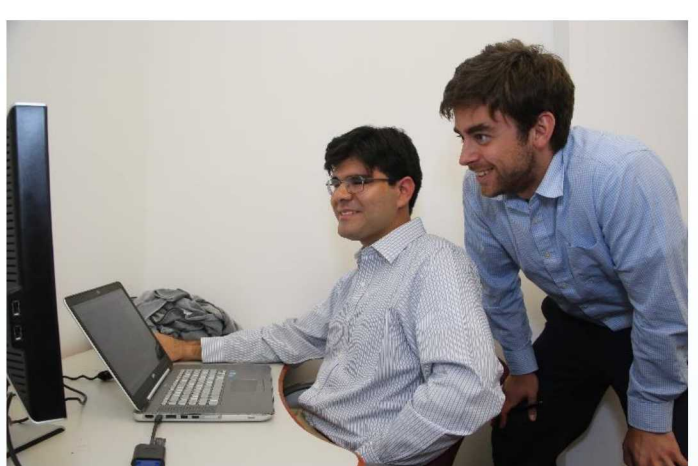
Overview / History

- Founded in 2014, NOMAD is a collaborative and educational research institute that unites graduate and undergraduate students to work on challenging research problems in engineering sciences
- Institute is co-hosted by Sandia National Laboratories and the University of New Mexico
- Inaugural year (2014) held at Sandia National Laboratories; 2015 and beyond held at the University of New Mexico Campus
- On average, each year has 6 projects consisting of 3 students and 2-4 mentors

Sandia
National
Laboratories

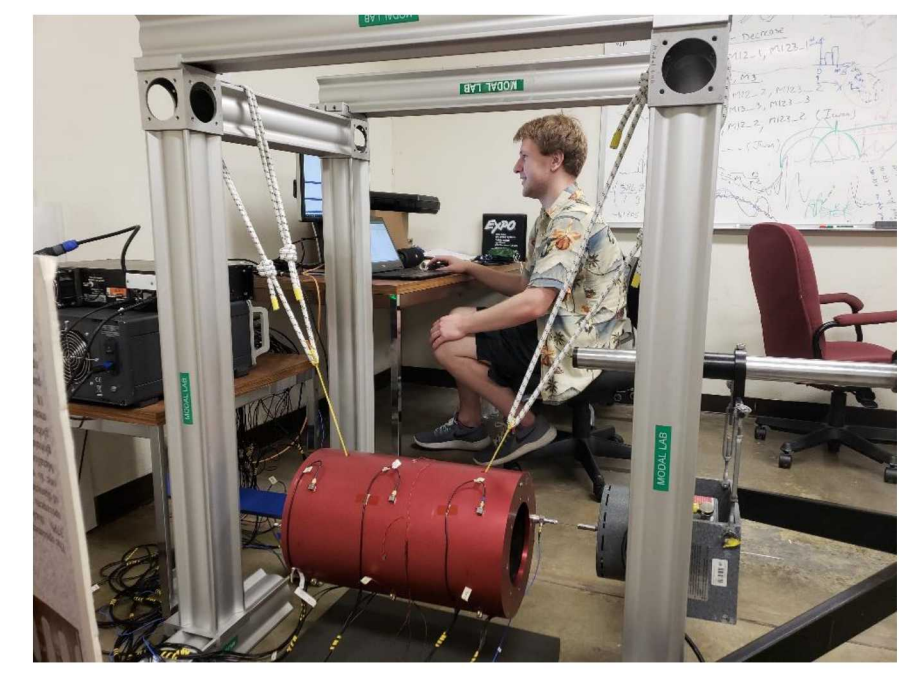
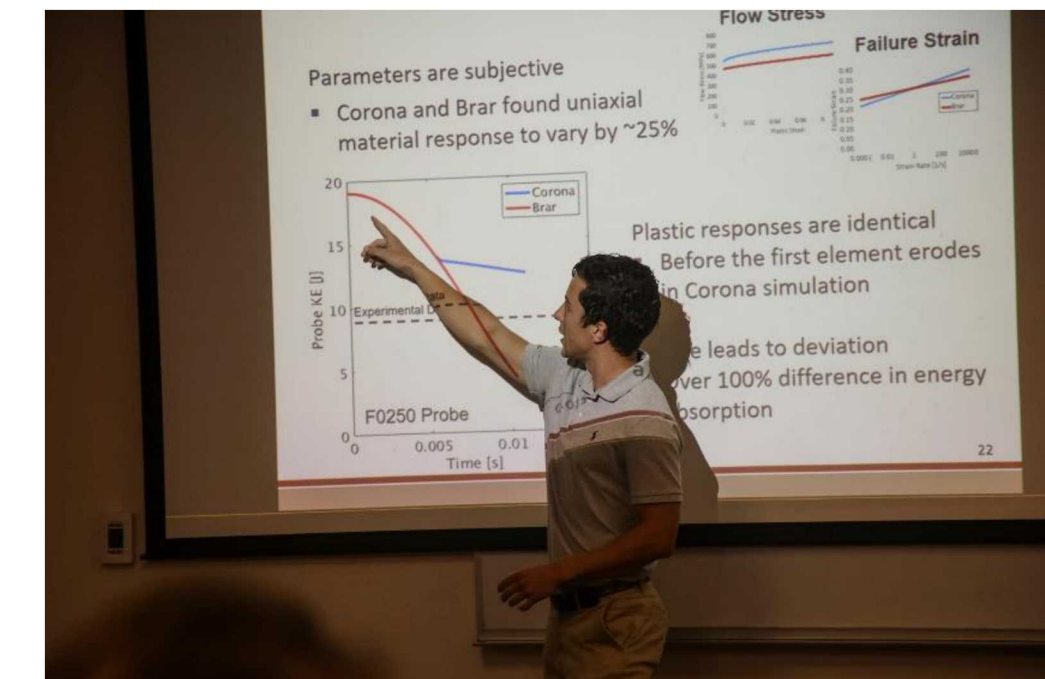
Impact

- Publish and present research in challenging fields of nonlinear mechanics and dynamics
- Ability to network and collaborate with researchers from around the world



2018 Highlights

- Research projects possessing experimental and computational aspects
- Weekly technical seminars on topics related to nonlinear mechanics and dynamics from visiting professors
- Organized social events including a night at an Albuquerque Isotopes baseball game
- Students presented research discoveries at the final NOMAD technical seminar



Path Forward

- Continue to improve external collaborations with greater research community by solving challenging research problems
- Develop strategic pipeline of highly qualified candidates to support national security mission
- Stewardship of novel technical advances to improve understanding of complex mechanical systems under extreme environmental loads

Contact Information

Visit our website at:

http://www.sandia.gov/careers/students_p_ostdocs/internships/institutes/nomad.html

Contact the organizers at:

nomad@sandia.gov

Achromatic, Varifocal Metalenses in the Visible Spectrum

Aiello, Maxwell D.*¹, Backer, Adam S.*², Sapon, Aryeh J.¹, Perreault, John³, Llull, Patrick³, Acosta, Victor M.¹



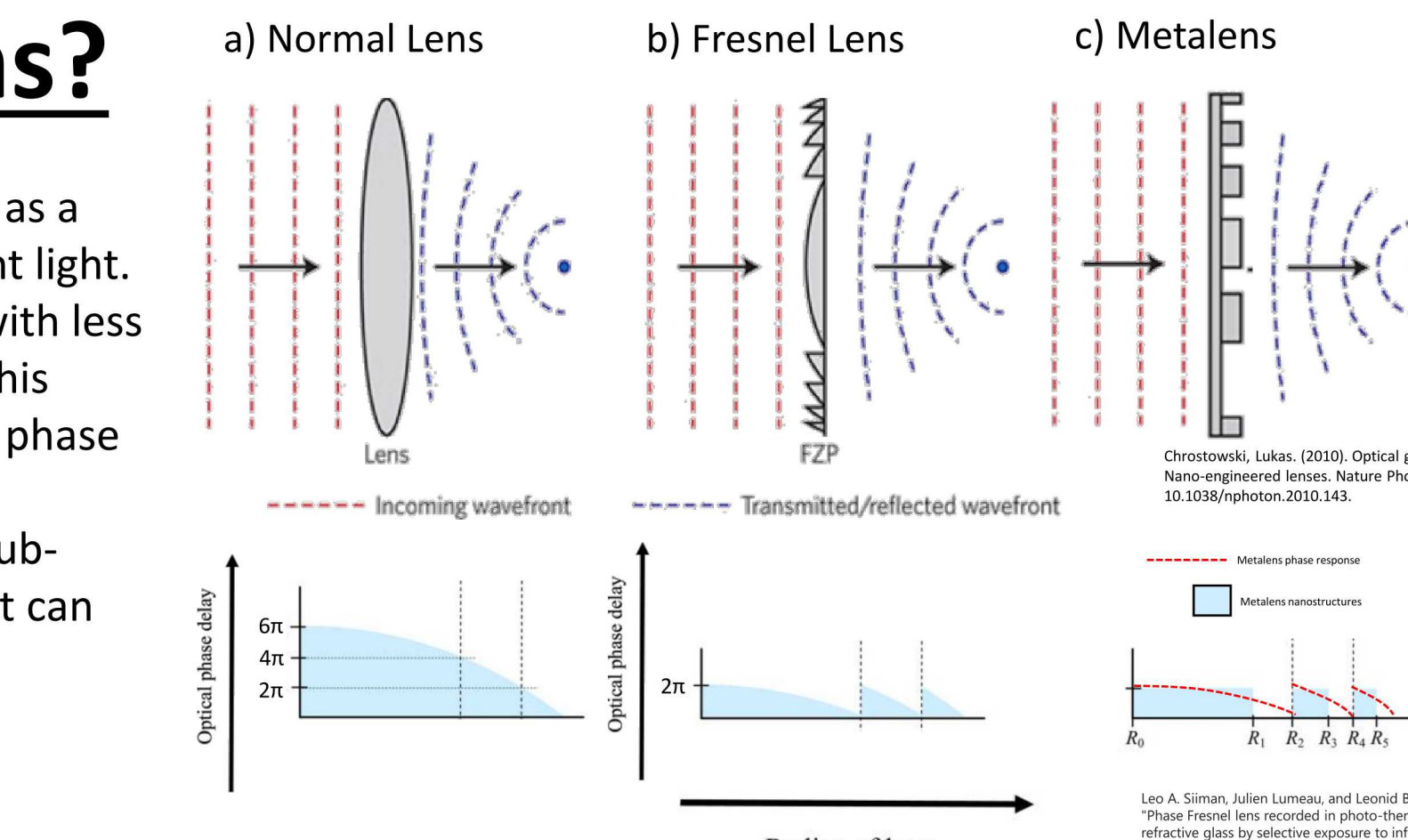
1. Center for High Technology Materials and Department of Physics and Astronomy, University of New Mexico, Albuquerque, NM 87106. 2. Sandia National Laboratories, New Mexico, P. O. Box 5800, Albuquerque, NM 87185. 3. Google Daydream, 1600 Amphitheatre Parkway Mountain View, CA 94043

*These authors contributed equally.

Introduction / Motivation

What is a Metalens?

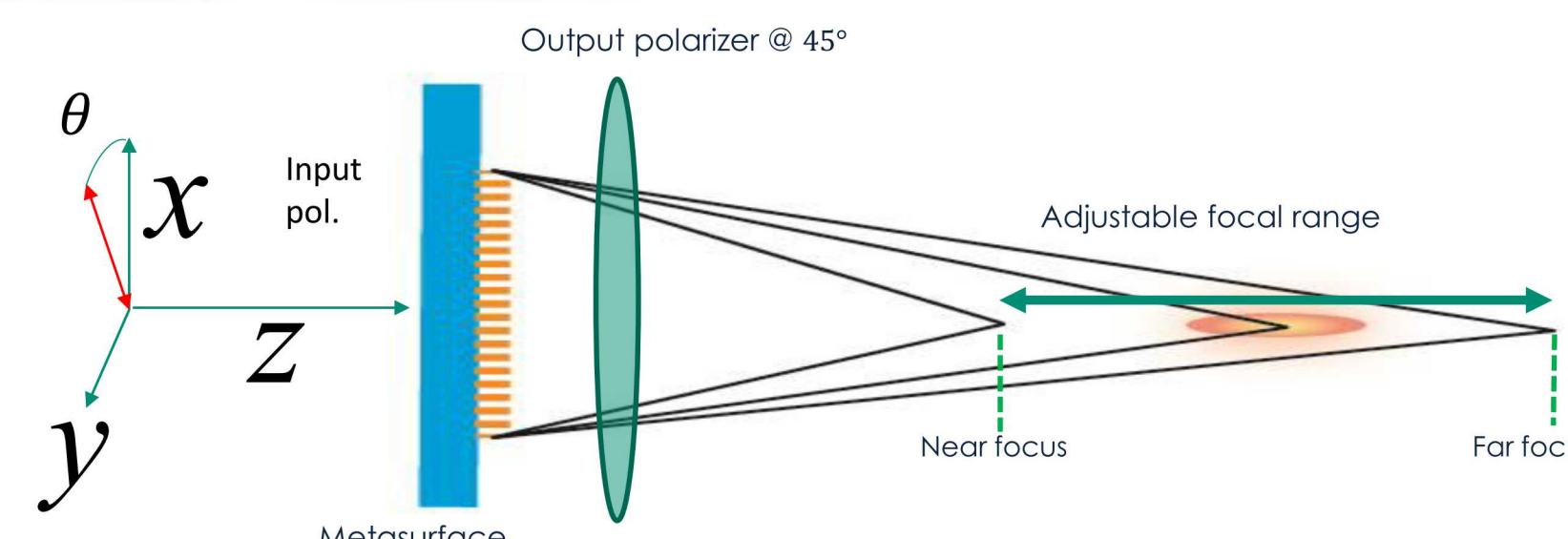
- a) A normal optical lens can be thought of as a parabolic phase manipulation of incident light.
- b) A Fresnel lens creates the same effect with less material by keeping the same slope of this parabolic phase and limiting the overall phase change to 2π .
- c) A Metasurface lens, i.e. Metalens, is a sub-micron thick, nanofabricated device that can mimic a lens and include additional functionality.



Goal of Project:

Demonstrate varifocal, Achromatic Metalenses for imaging/display

- Vary the linear input polarization from 0° to 180° to vary the focal length of the Metalens



Challenges

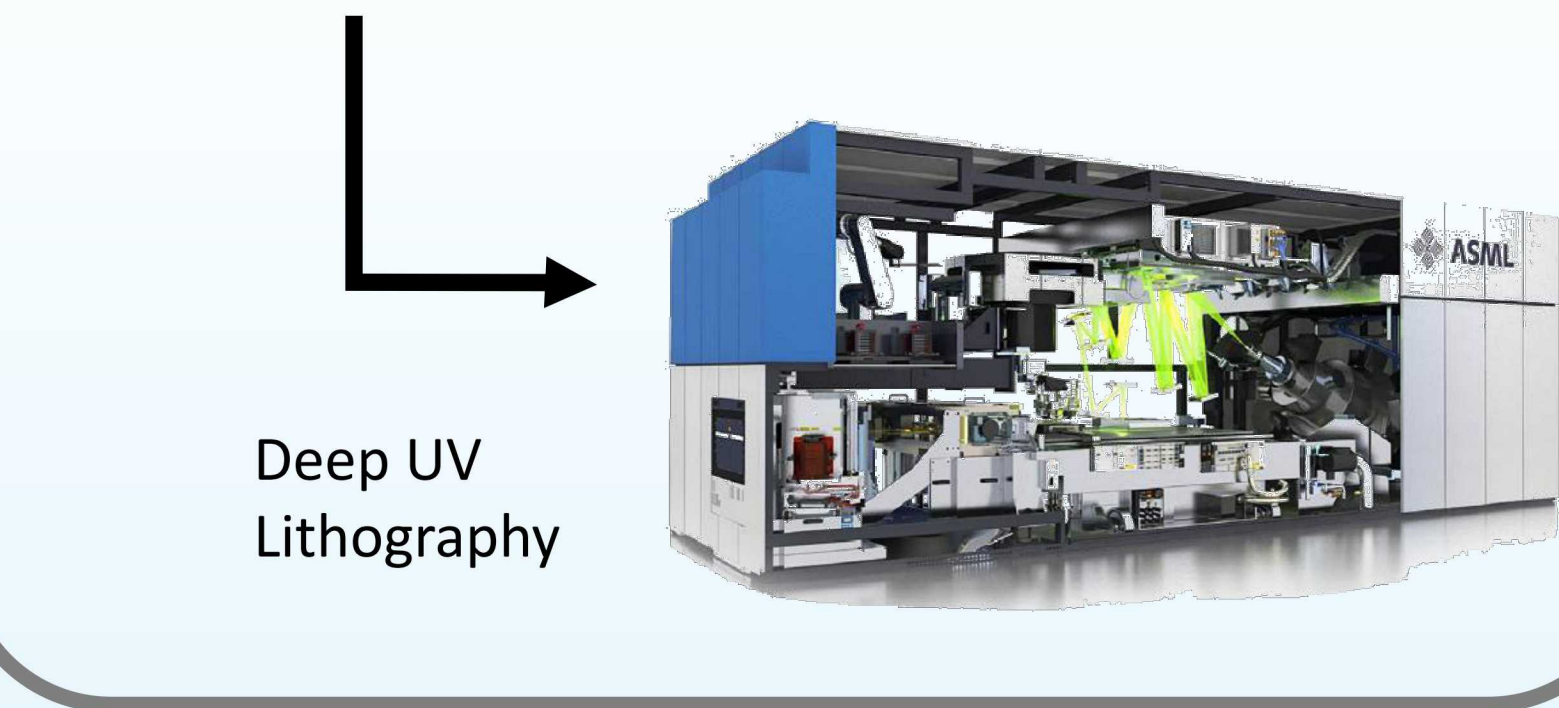
Scaling

- Electron beam lithography does not scale well to larger diameter optics.
- Need to transition to a mask-based photolithography scheme for rapid fabrication.



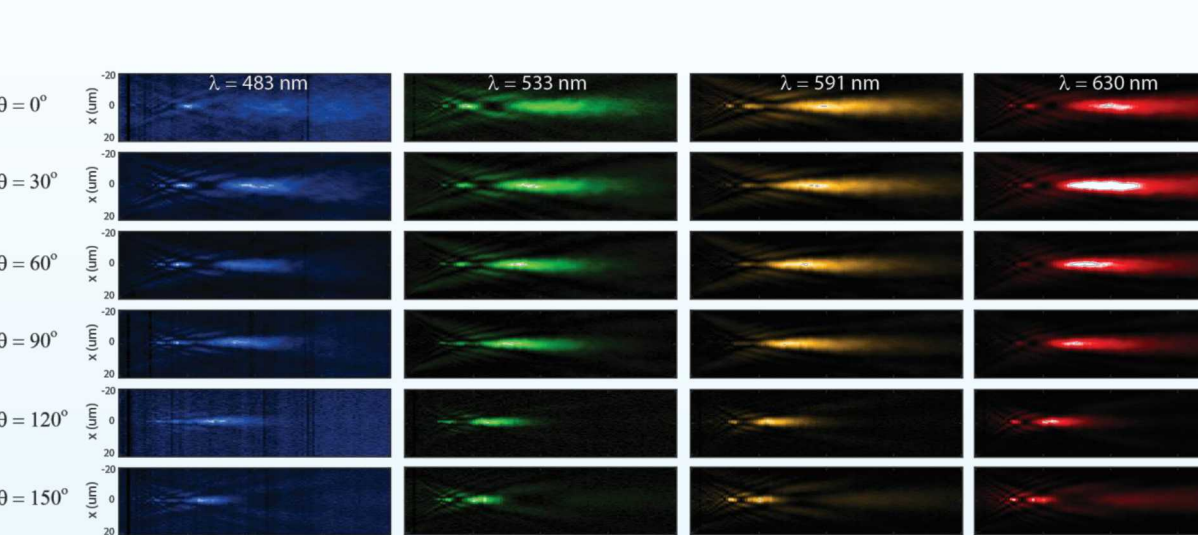
Electron Beam Lithography

Deep UV
Lithography



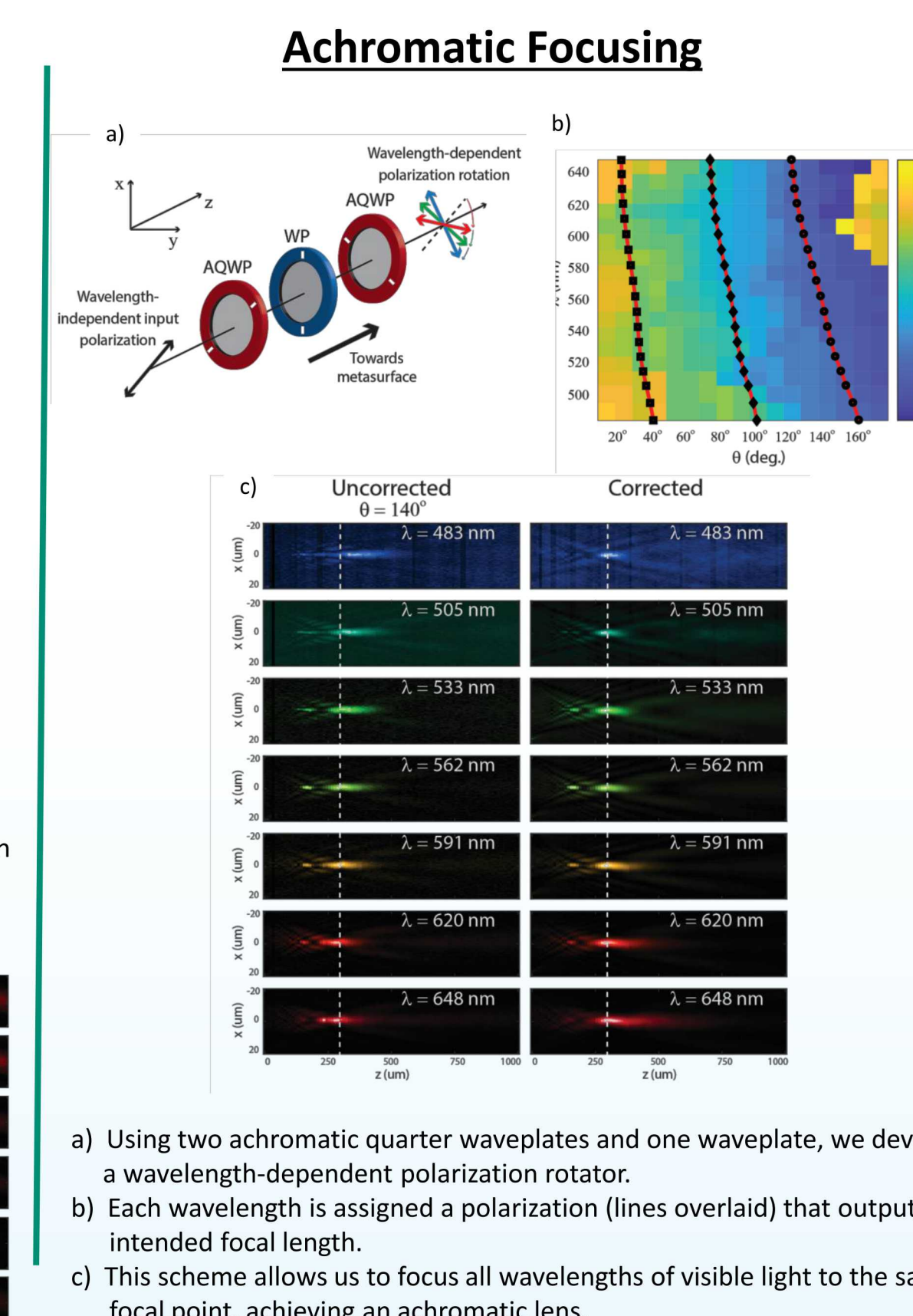
Optical Characterization

Above: Our characterization setup allows full control of wavelength and polarization of light incident on Metasurface. In addition, we scan in the z -direction to capture the focus of the Metalens.
Below: XZ-slices of the Metalens PSF. Focal-length characterized as a function of wavelength and polarization.



Results

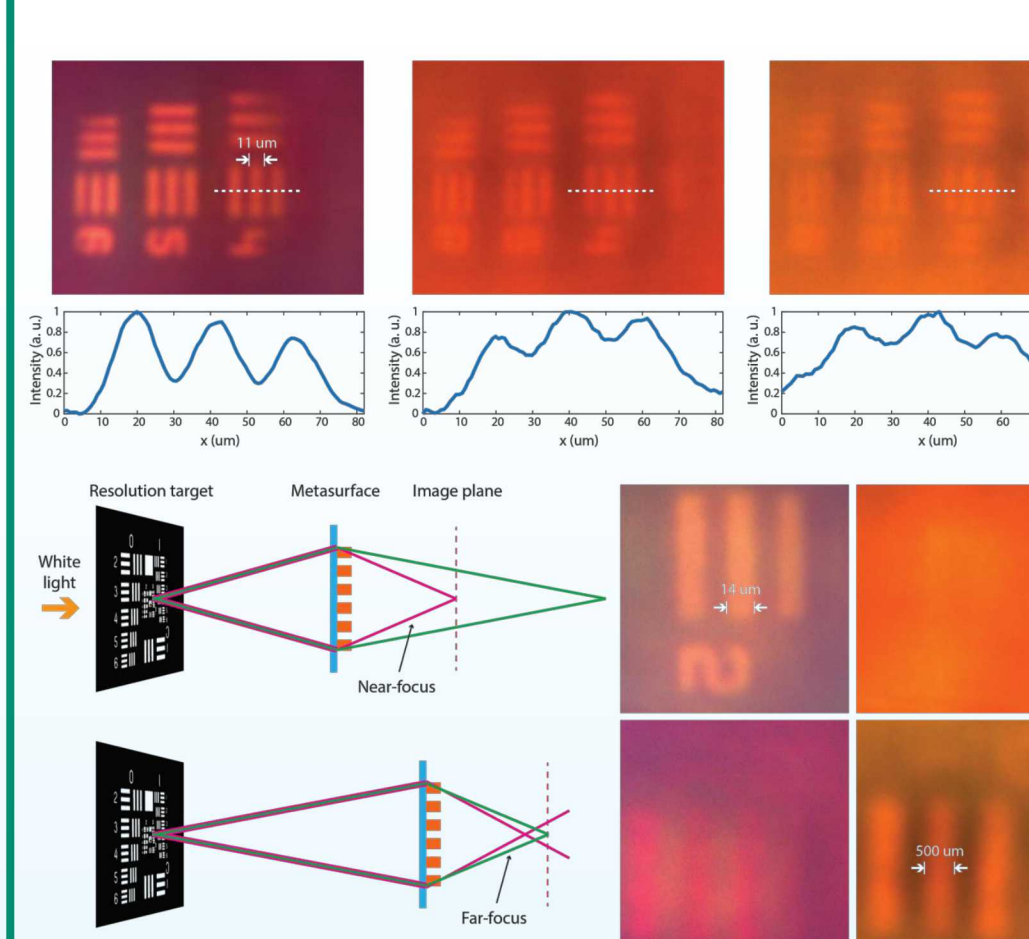
Achromatic Focusing



- a) Using two achromatic quarter waveplates and one waveplate, we develop a wavelength-dependent polarization rotator.
- b) Each wavelength is assigned a polarization (lines overlaid) that outputs an intended focal length.
- c) This scheme allows us to focus all wavelengths of visible light to the same focal point, achieving an achromatic lens.

Broadband Imaging

- Image-capture using white light proves the effectiveness of our Metalens.
- Imaging a standard 1951 USAF resolution target we can see: **top:** the resolution as a function of different focal settings. **bottom:** Polarization-based refocusing.



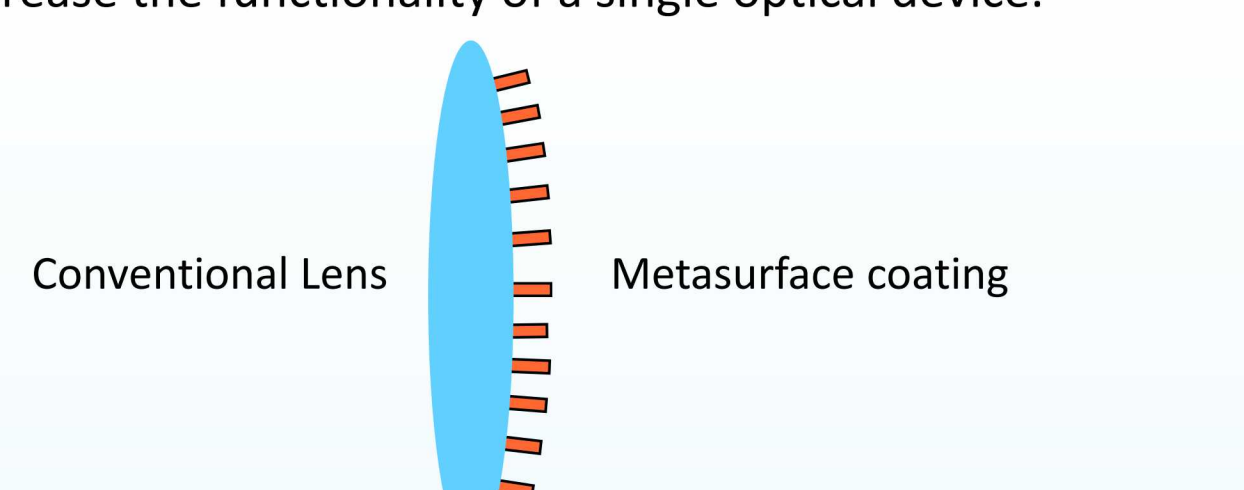
Partnerships

Collaborations

- This work was completed in collaboration with Google Daydream for a Virtual/Augmented Reality display application.
- The work was completed as a joint UNM and Sandia National Laboratories effort. Adam Backer acknowledges research support from the Harry S. Truman Fellowship.

Future Work

- Patterning Metasurfaces onto conventional optics to further increase the functionality of a single optical device.



- Use computational inverse-design techniques to develop non-intuitive optimized metasurfaces.

Irradiation Resistance of Interfaces in Zr–Nb Nanocomposites

Elton Chen^[1,2], Rémi Dingreville^[1], Chaitanya Deo^[2]

[1] Center for Integrated Nanotechnologies, Sandia National Laboratories

[2] G.W. Woodruff School of Mechanical Engineering, NRE Program, Georgia Institute of Technology



Introduction / Motivation

- Grain and phase boundaries act as defect sinks and barriers, subsequently strengthen the material by governing different deformation mechanisms like interfacial shearing, dislocation nucleation and motion, and interfacial-driven twining.
- Nano-laminate composites are engineered to take advantage of these boundary effects and further extend material mechanical performance.
- Exposure to irradiation and other external factors can change phase boundary structures, compositions, and properties.
- Mechanical performance degradation can be tied to microstructural change at/near the phase boundaries.

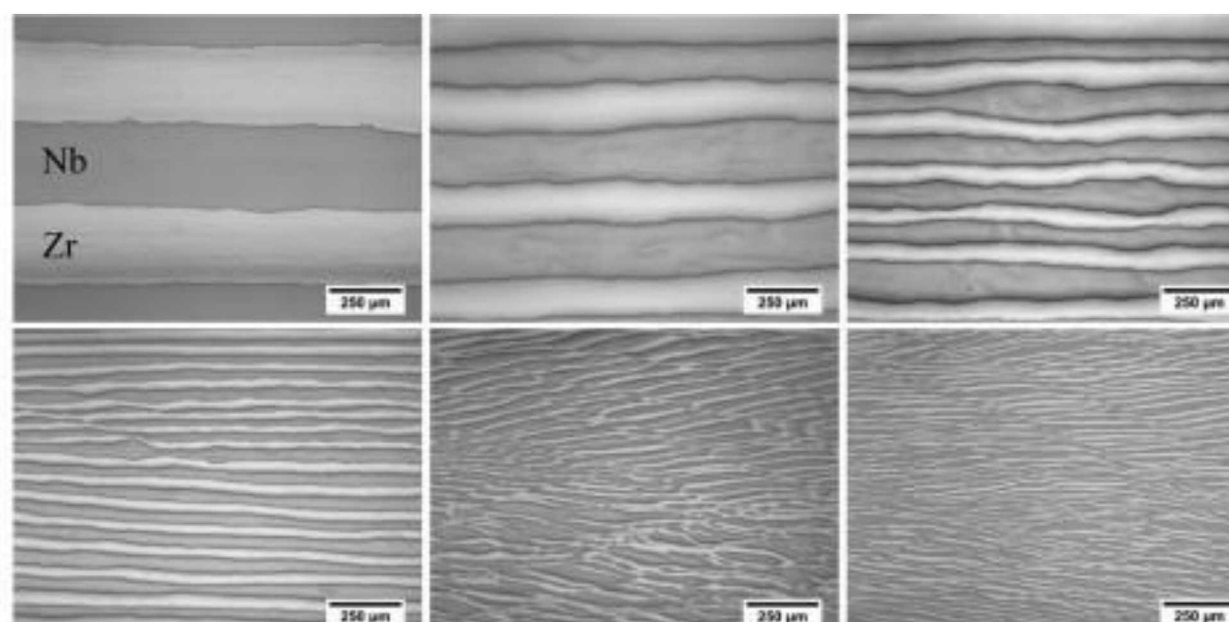


Figure 1: Rolling manufactured Zr-Nb laminar composites. [1]

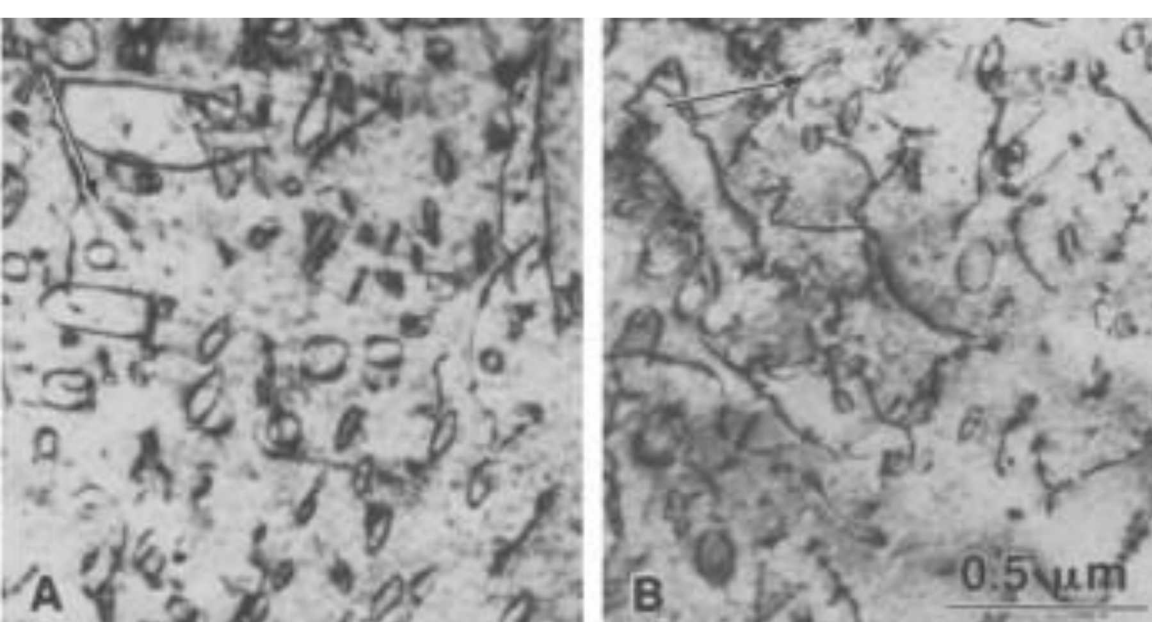


Figure 2: Irradiated dislocation loop in bulk Zr. [2]

- Molecular Dynamics (MD) is the best method of simulating irradiation defect accumulation at the atomic size-scale.
- Each radiation event is represented by a series of atom-atom collision events combined into a larger displacement cascade.
- Simulation of full displacement cascades is too slow and computationally expensive for high dose level.
- Permanent radiation damage are directly introduced as vacancy-interstitial (Frenkel) pairs by atomic displacement. [3]
- Accelerated defect implantations allow access to high dose damaged states.
- Simulation is relaxed intermittently to allow for defect structure evolutions.
- Initial nano-laminate composites are constructed by rotating and stacking Zr and Nb bulk crystals with structured interfaces.

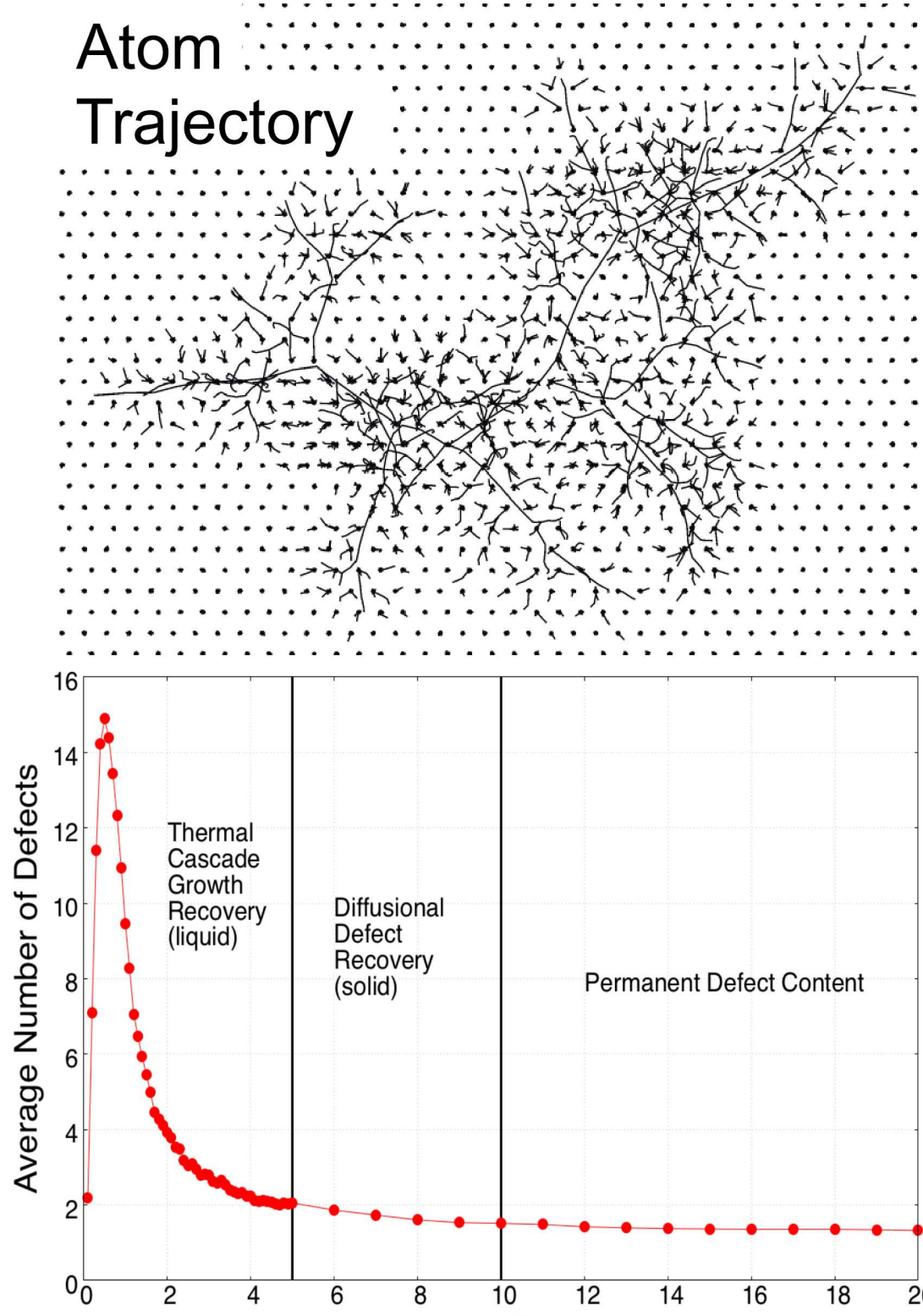


Figure 3: Radiation cascade development & defect population.

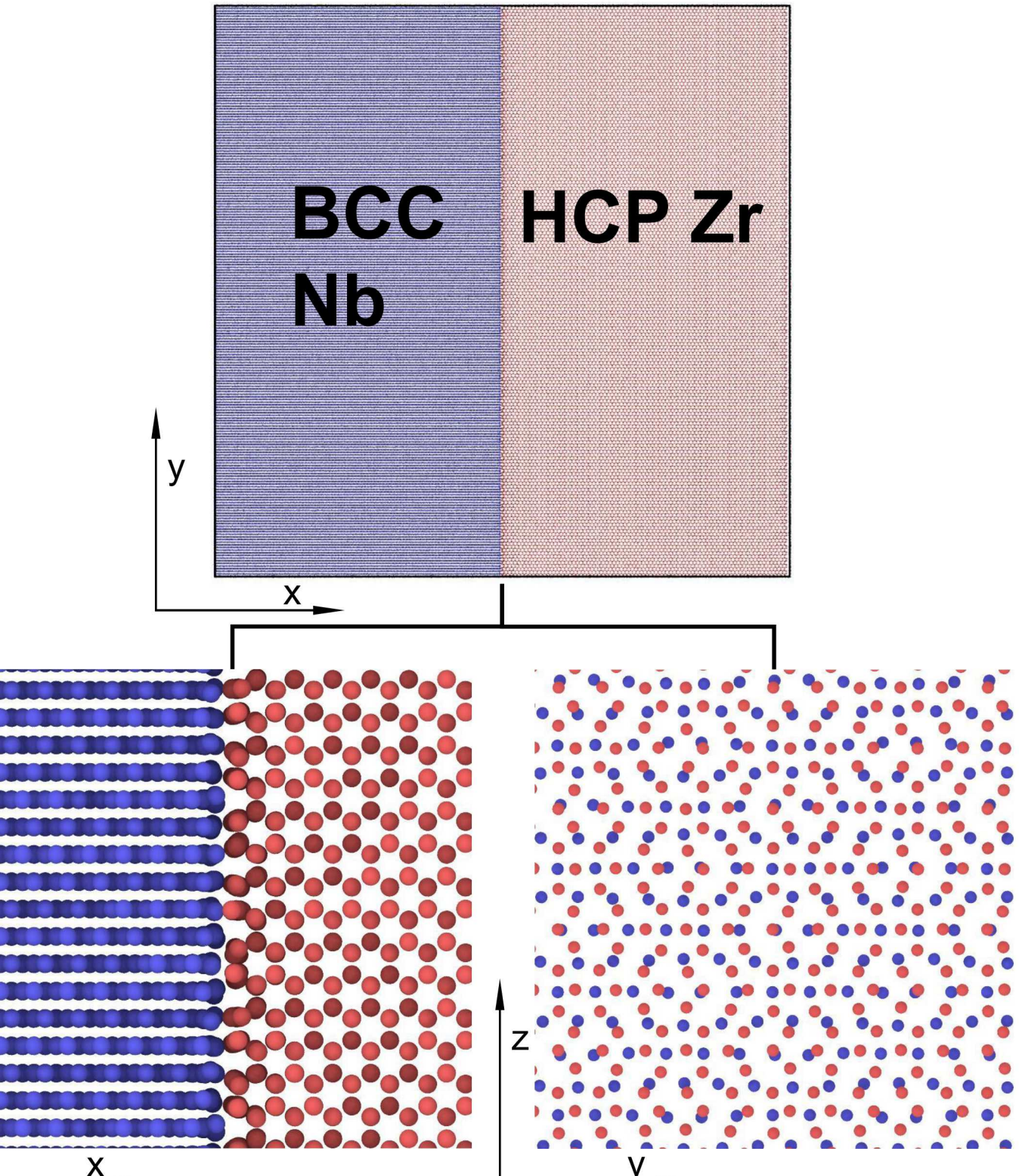


Figure 4: Zr-Nb laminate composite & interfacial microstructure.

Results

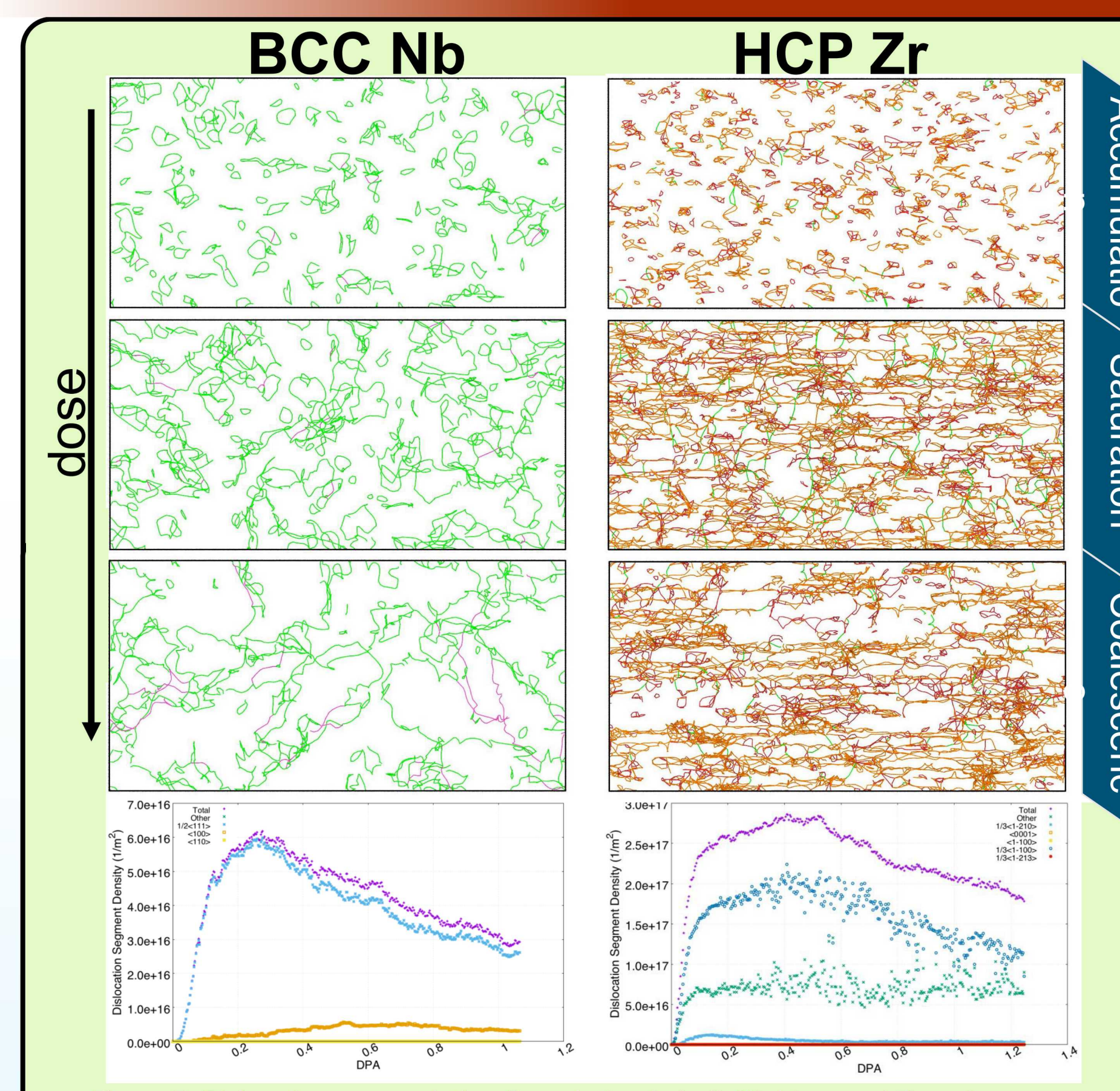


Figure 5: Dislocation accumulation & evolution in bulk Niobium and Zirconium.

Bulk Crystalline

- Three stages of defect accumulation:
 - Small dislocation accumulation
 - Dislocation saturation
 - Coalescence to large dislocations
- Formation of larger dislocation loops decreases the overall dislocation density.
- HCP Zr dislocation formations match those observed from electron radiation experiments.

Nano-laminate Composite

- A secondary rise in dislocation density exists in the BCC sub-layer.
- Increase in dislocation density corresponds to trapping of smaller BCC dislocation loops near the phase boundaries.
- Composition mixing near the boundary induces HCP \rightarrow BCC phase transition and dislocation trapping.

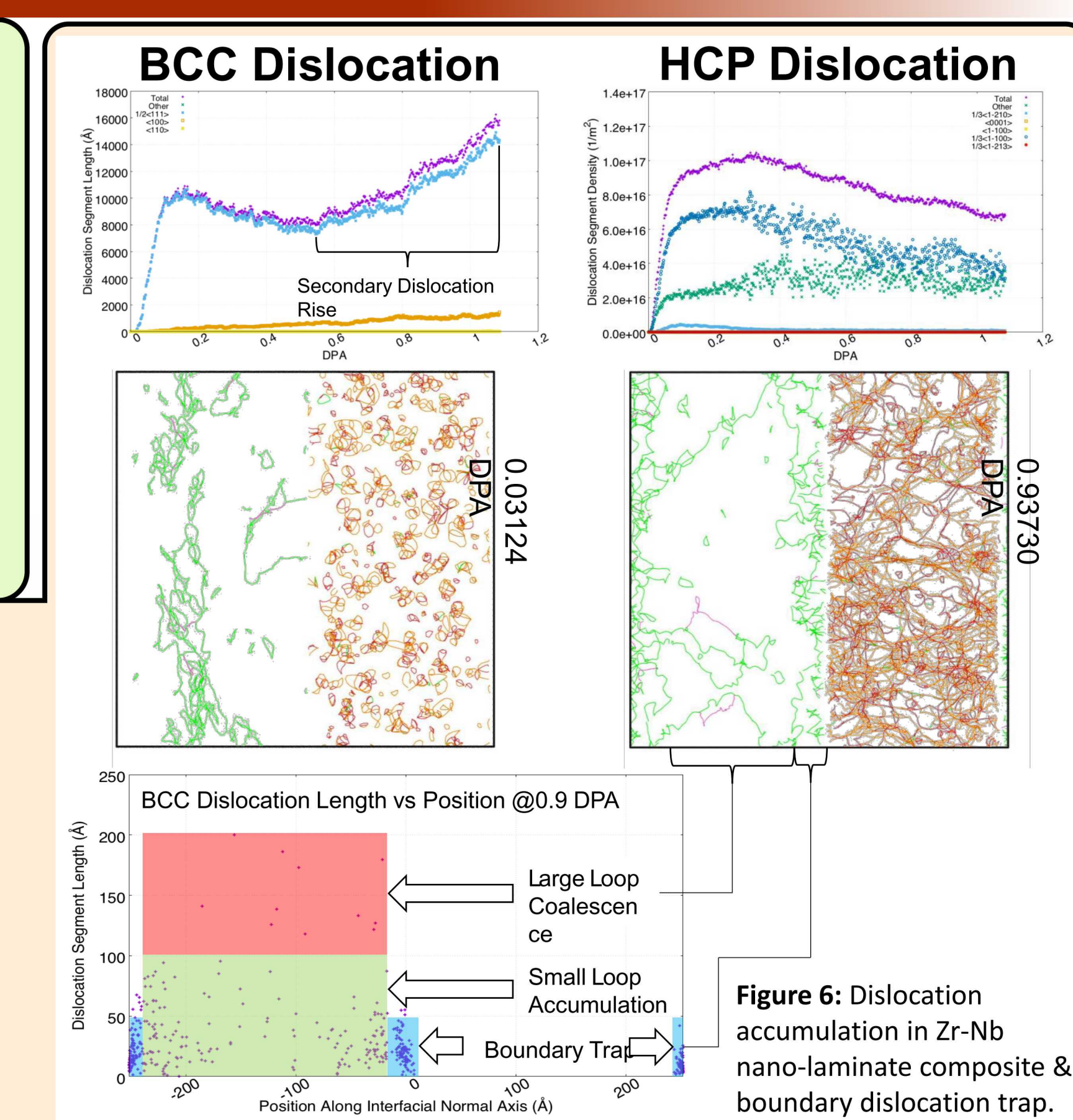


Figure 6: Dislocation accumulation in Zr-Nb nano-laminate composite & boundary dislocation trap.

Partnerships

- Improving the radiation damage accumulation model by introducing new dose rate and dose type effects.
- Evaluating the radiation effect on mechanical performance through fracture simulations of the irradiated nano-laminate composites.

This work was performed in part at the Center for Integrated Nanotechnologies, an Office of Science user facility operated for the U.S. Department of Energy. The authors acknowledge the support from the Woodruff Faculty Fellowship at Georgia Institute of Technology, and the Sandia Laboratory Directed Research and Development (LDRD) Academic Alliance program.

- [1] Knezevic, Marko, et al. "Texture evolution in two-phase Zr/Nb lamellar composites during accumulative roll bonding." *International Journal of Plasticity* 57 (2014): 16-28.
- [2] Choi, Sang Il, and Ji Hyun Kim. "Radiation-induced dislocation and growth behavior of zirconium and zirconium alloys—a review." *Nuclear Engineering and Technology* 45.3 (2013): 385-392.
- [3] Chartier, A., et al. "Early stages of irradiation induced dislocations in urania." *Applied Physics Letters* 109.18 (2016): 181902.

Refractive Imaging of Microscale Defects in PETN Films

Julio C. Peguero, Eric C. Forrest, Michael J. Hargather, Robert Knepper, Alexander S. Tappan, Michael P. Marquez, Jonathan G. Vasiliauskas, and Stephen G. Rupper



Introduction / Motivation

Physical vapor deposition (PVD) is used to produce explosives with great control over the morphology and microstructure. Deposition of densified PETN films is possible by depositing onto substrates with high surface energy. However, the densified films suffer from micro cracking throughout, as shown in Figure 1, because of residual thermal stresses caused by a mismatch of thermal expansion coefficients between the substrate and the PETN. To simulate the effects of the micro cracking, gaps are engineered by separating two films by a known width as shown in Figure 2. Refractive imaging is used to observe the shock front shape to determine if the detonation propagates across each gap thickness.

Figure 1. Densified PETN film displaying micro cracking

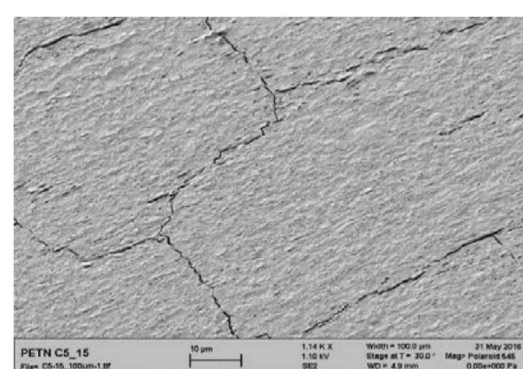


Figure 2.
Top down view of gap test structure

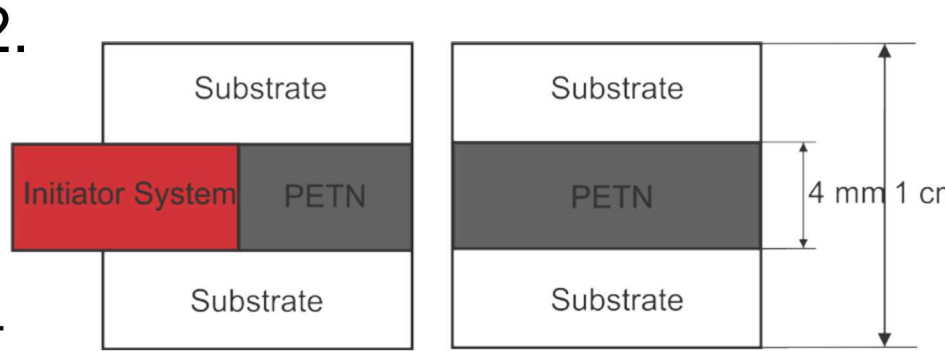


Figure 2. Top down view of gap test structure

Approach

Refractive imaging was used to visualize shock waves in air produced by the detonation of the PETN films. The primary imaging method was a “focused” shadowgraph technique. Focused shadowgraph is used to visualize the second derivative of the refractive index. A detailed schematic of a focused shadowgraph system is shown in Figure 3.

The shock front was tracked using a custom developed image processing routine. The shock tracking was done with a Canny filter, and then a mask was applied to remove noise that was inadvertently picked up with the Canny filter. The approach ultimately resulted in an image of the shock front location. The shock front was automatically extracted from the binary image for each pixel row in the image. The pixel location was converted to a spatial location using a calibration grid with known spacing. Velocities are calculated from successive shock wave positions using a backward finite difference method. Where appropriate, centered differences were used for steady state shock wave propagation.

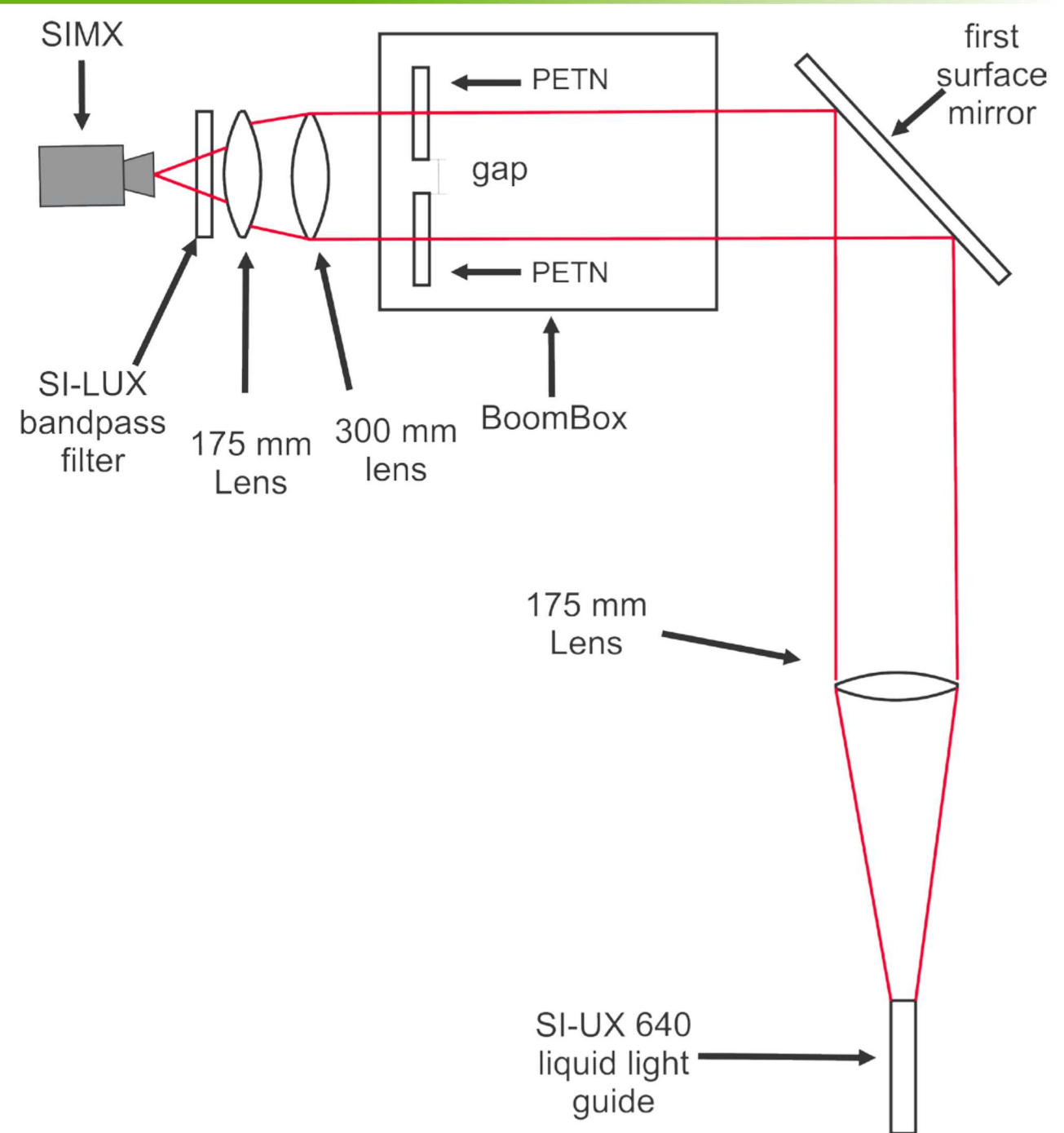


Figure 3. Focused shadowgraph system used during testing.

Results

Thought the test series, the critical gap width for reliable detonation of a 200 μm thick film was found to be approximately 75 μm . Detonation across a gap larger than 80 μm was observed in one instance. The tests with successful propagation exhibit a deceleration of the shock front and then return to steady state as shown in Figure 4. When the gap is large enough detonation fails to propagate, and the shape of the shock front goes from roughly linear in shape to roughly circular in shape as shown in Figure 5.

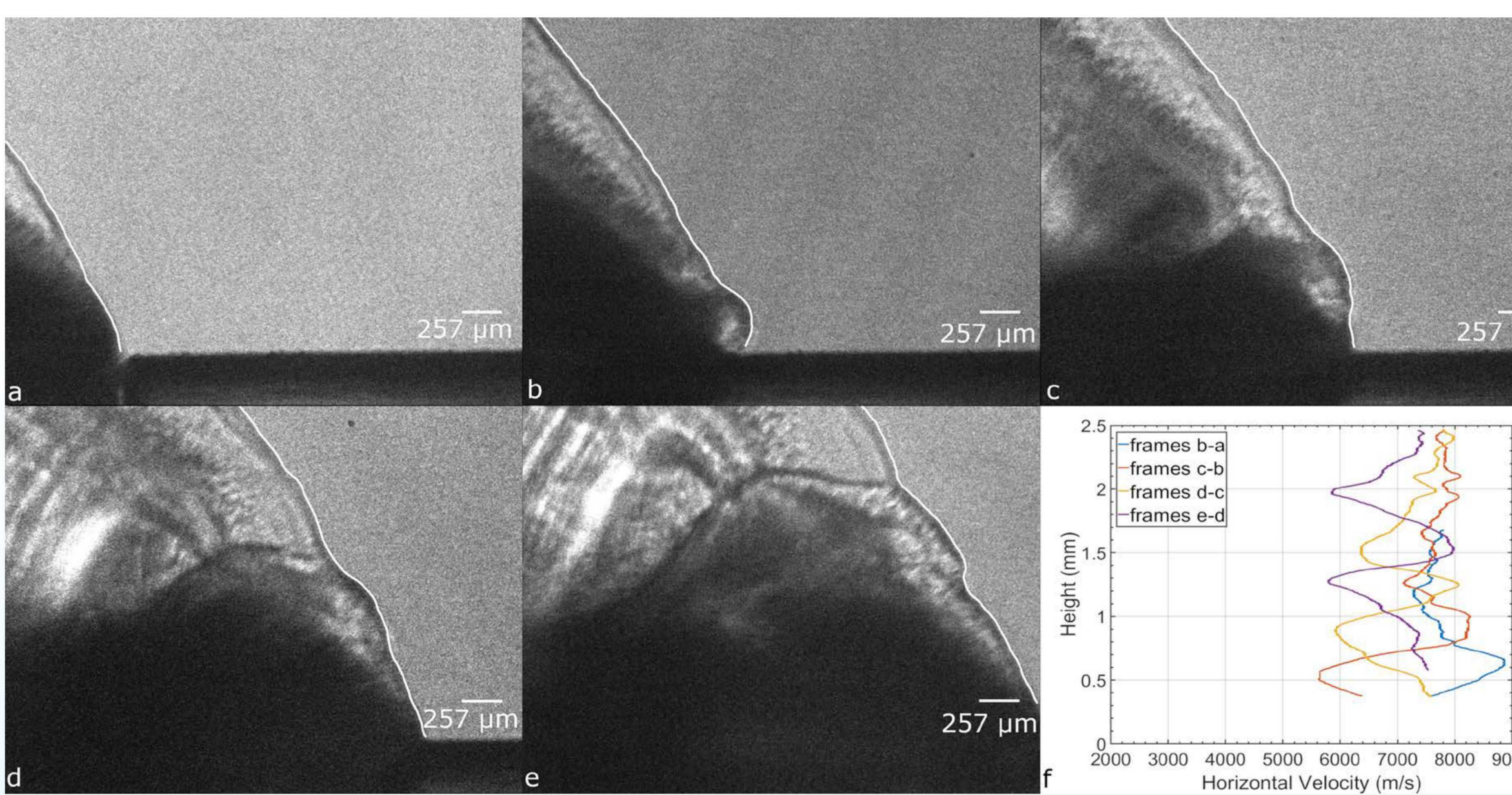


Figure 4. (a)-(e) Propagated shot, 90 ns between frames. (f) Backward difference horizontal velocity for frames above.

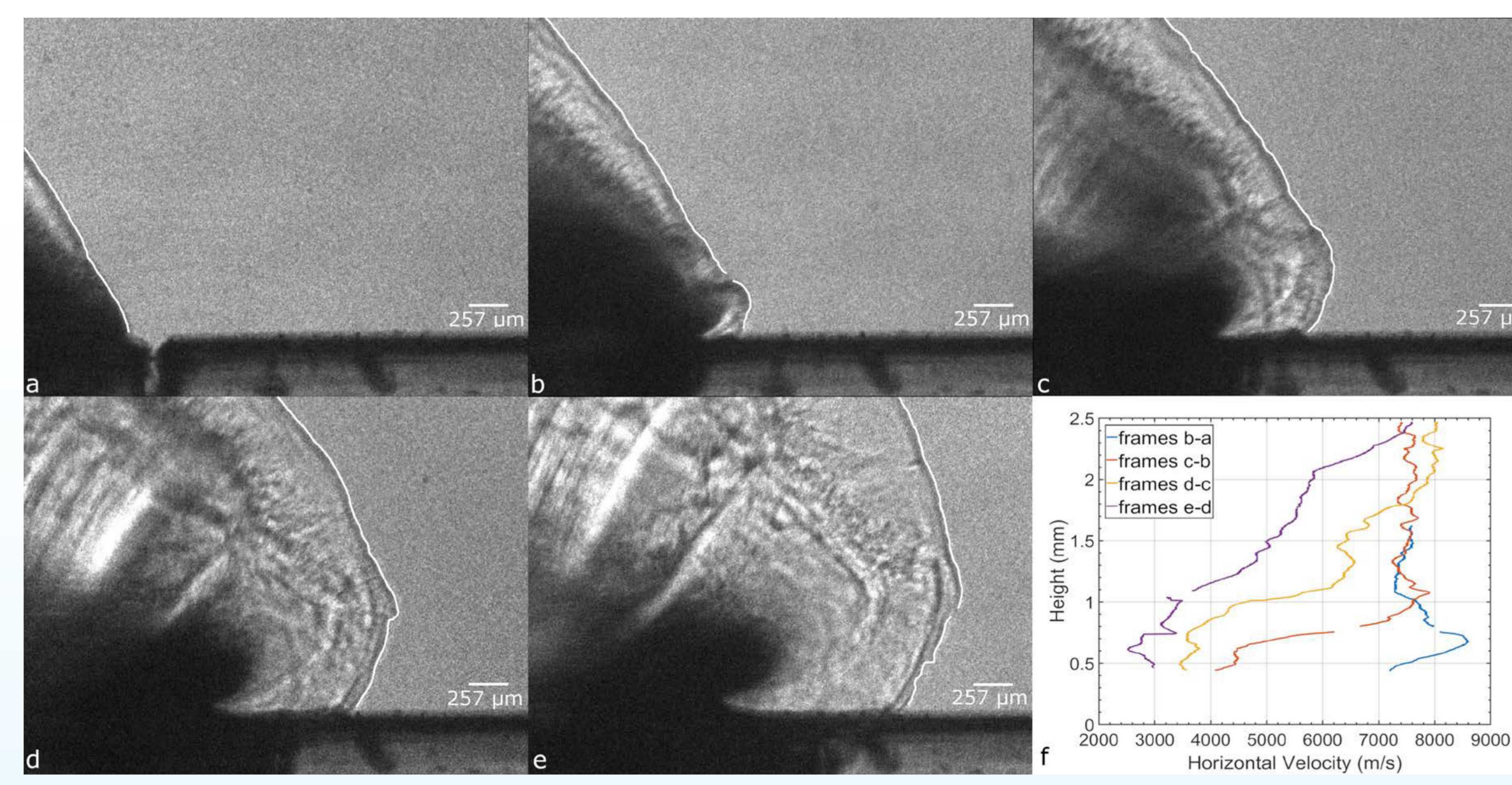


Figure 5. (a)-(e) Failed shot, 100 ns between frames. (f) Backward difference horizontal velocity for frames above.

Future Work

Implementation of velocity measurements normal to the shock front is currently in development. This is achieved by matching a point on a shock front to the point in the normal direction on the subsequent shock front. An example is shown in Figure 6.

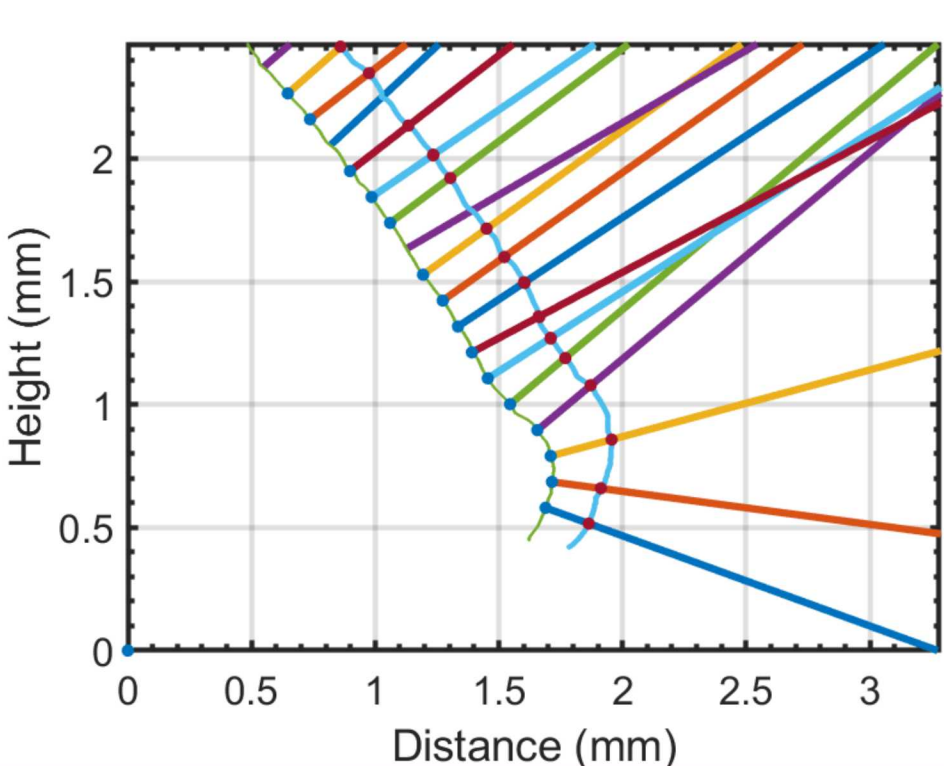


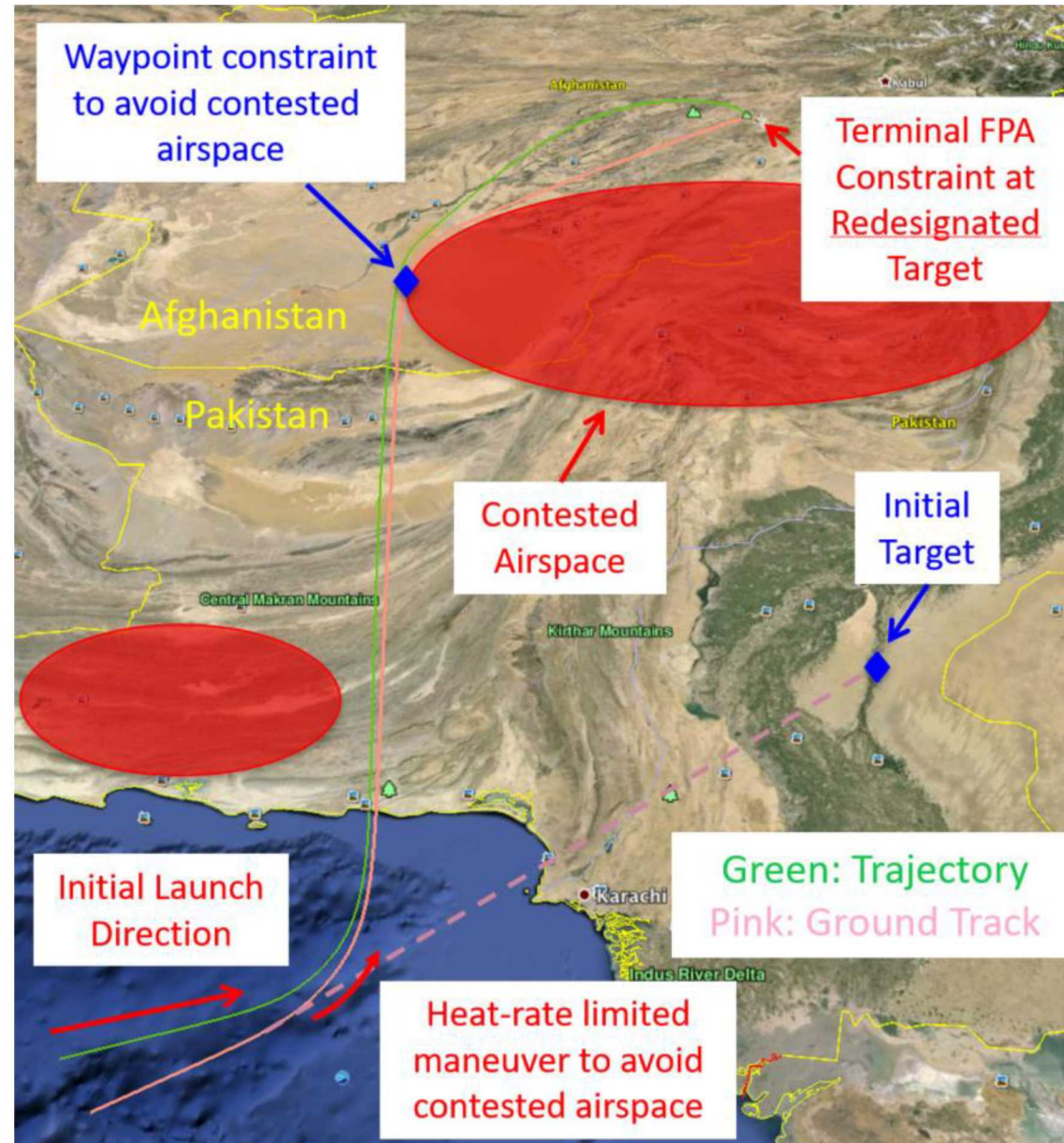
Figure 6. Current state of normal point matching. The line connects a point on the original shock front to two possible matches on the second shock front.



Objective

Rather than flying preprogrammed trajectories, create a **rapid** and **reliable** “full flight” **guidance algorithm** that can update the desired flight path in an **optimal manner** based on external factors or changes to the mission

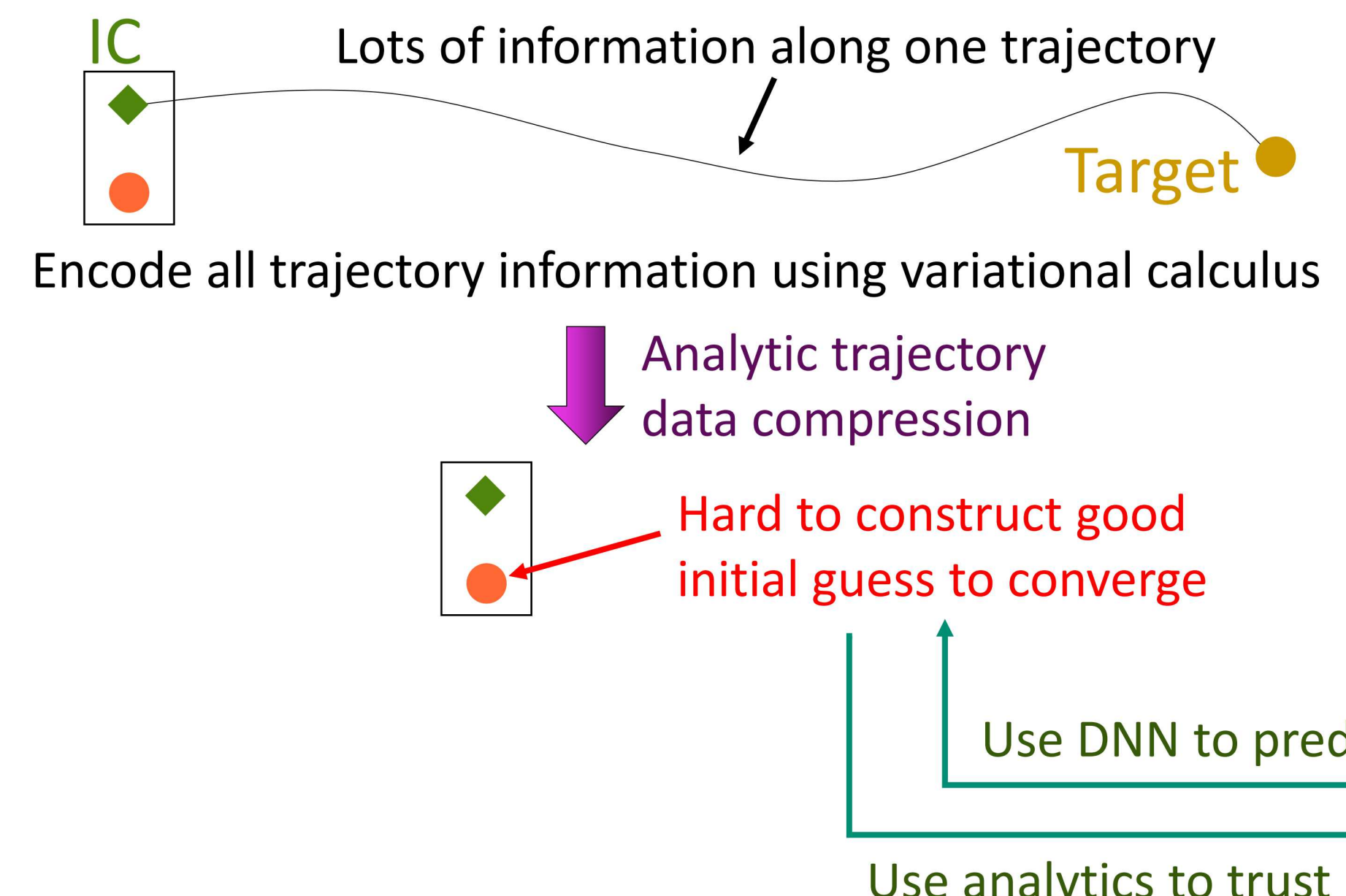
- Combine classical optimization methods for dynamical systems with machine learning



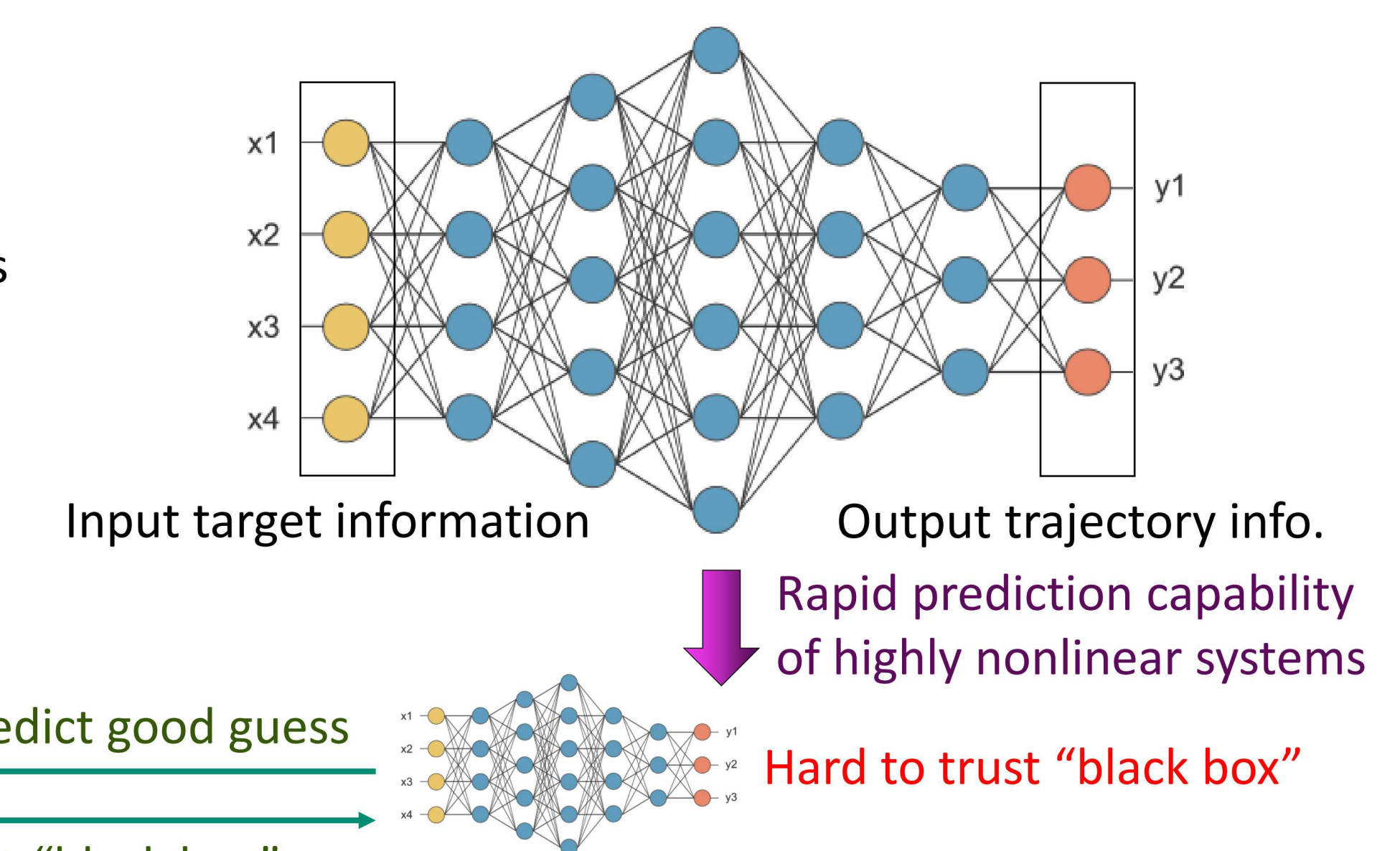
Test classical optimization/machine learning algorithm on representative flight hardware

Approach

Classical Physics-Based Optimization



Modern Big Data/Machine Learning



- **Expected to significantly reduce or eliminate iteration** associated with traditional guidance techniques
- **Partner with Maruthi Akella (Aero. Eng. at UT Austin)** on numerical stabilization techniques

Challenges

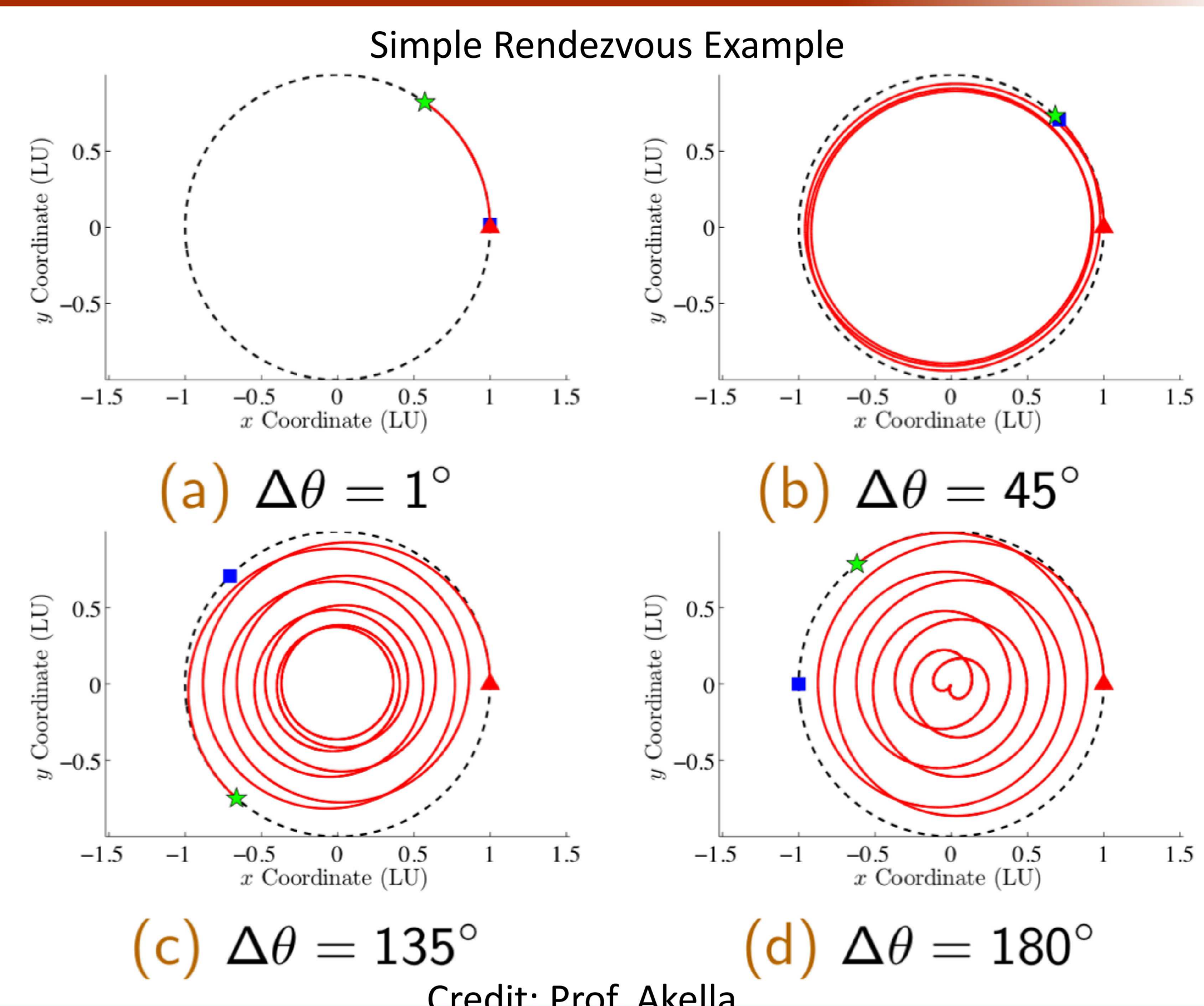
Converging to solutions, even with intelligent initial guesses from machine learning algorithms, **can be challenging**

- High sensitivities
- Numerical difficulties

Research by Prof. Maruthi Akella has focused on **numerical stabilization techniques** that will **improve the robustness** of the overall process

- Research expected to significantly **increase the confidence of converging to solutions** during flight
- Approach **may also increase speed of convergence to solutions**

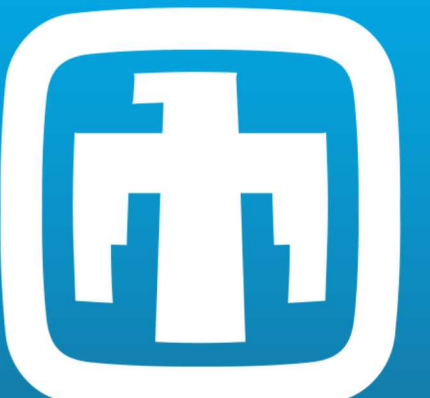
Results



Partnerships

Prof. Akella's research includes complimentary work in **finite time Lyapunov controllers** that guarantee convergence to feasible solutions

- Can serve as a **backup** to construct solutions in the **unlikely event** that the **numerical stabilization** technique fails
- Backup solutions expected to be **similar to optimal solutions** obtained from machine learning
 - Serve as **temporary feasible trajectories** until primary method reestablishes trajectory solutions

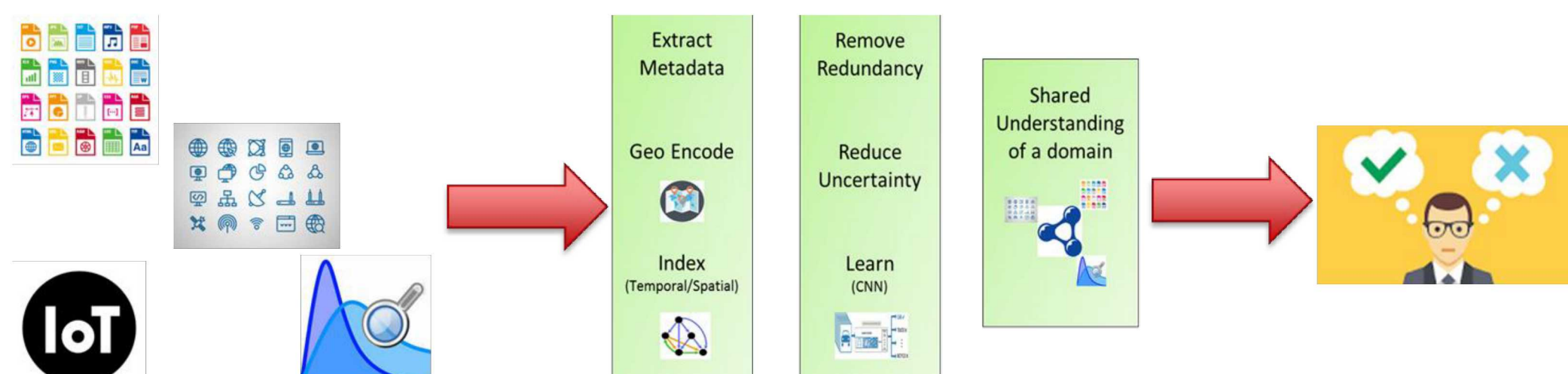


Turning Big Data into Actionable Intelligence

Tian Ma, Rudy Garcia, Forest Danford, Laura Patrizi, Jenny Galasso, Tim Draelos, Thushara Gunda, Jason Loyd, Otto Venezuela, Wesley Brooks

Introduction / Motivation

- Significant increase in amount of digital information
 - “90% of the data in the world today has been created in the last two years alone, at 2.5 quintillion bytes a day” – IBM Marketing Cloud (December 2016)
 - There are more data than human can analyze
- Data are “Gold” only if you can uncover an insight
- Quickly turn real-time streaming data from variety of sources into actionable insights that enables decision makers from political leaders to field commander to take appropriate action when faced with security threat

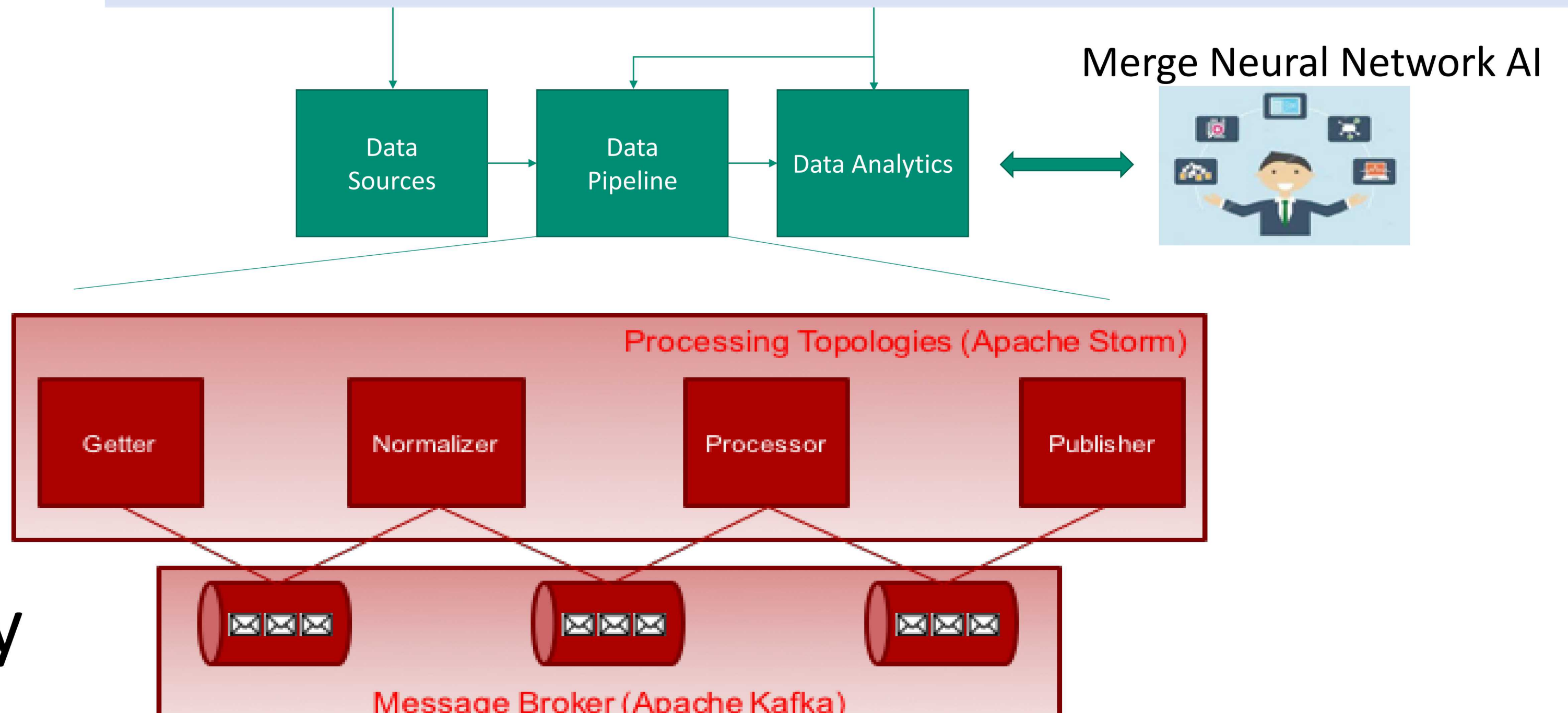


Approach: Big Data Actionable Intelligence Architecture

Twitter: Tweets around Chicago: ~125k tweets / day
TravelMidwest: Tweets filter on traffic keywords and emojis
City of Chicago: Web Camera Images: ~20k / day
 Vehicle Detection System readings: ~30k / day
 Dynamic Message Sign records: ~20k / day
 Traffic Segments : ~120k records / day
MapQuest: Traffic Region: ~4k records / day
 Construction Moratorium: ~1000 / day
 ~ 50 incidents / day
Digital Globe: Satellite Imagery ~ 1 image every 2-3 days
 Dash Camera Video (2-3 videos max)

~300k records / day

Data normalization allows meaningful comparisons of events in space, time, and context

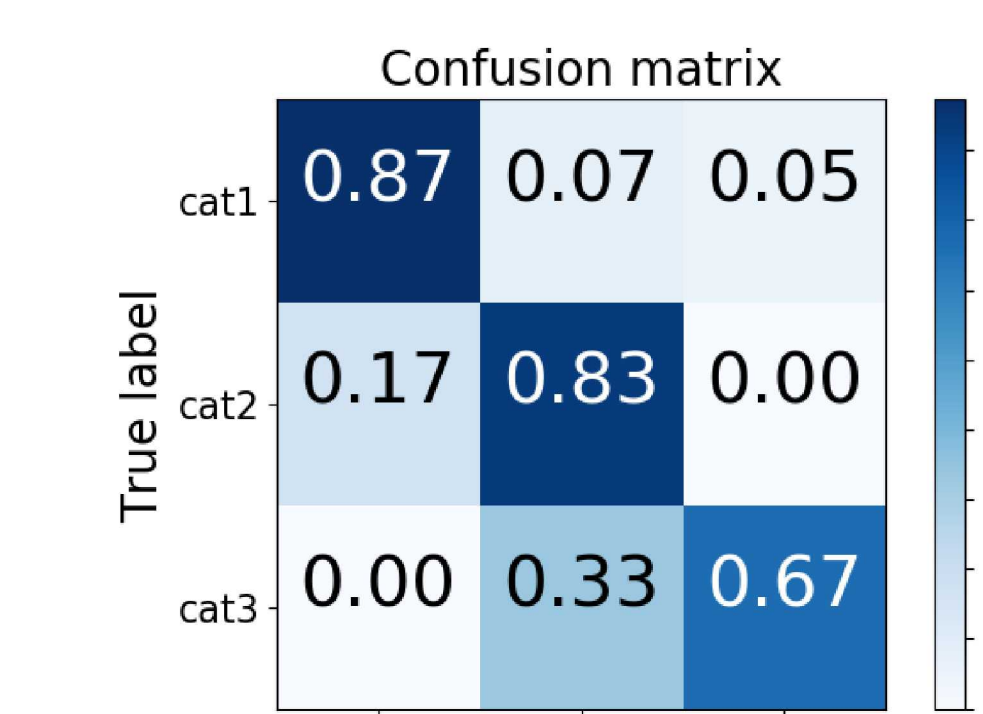
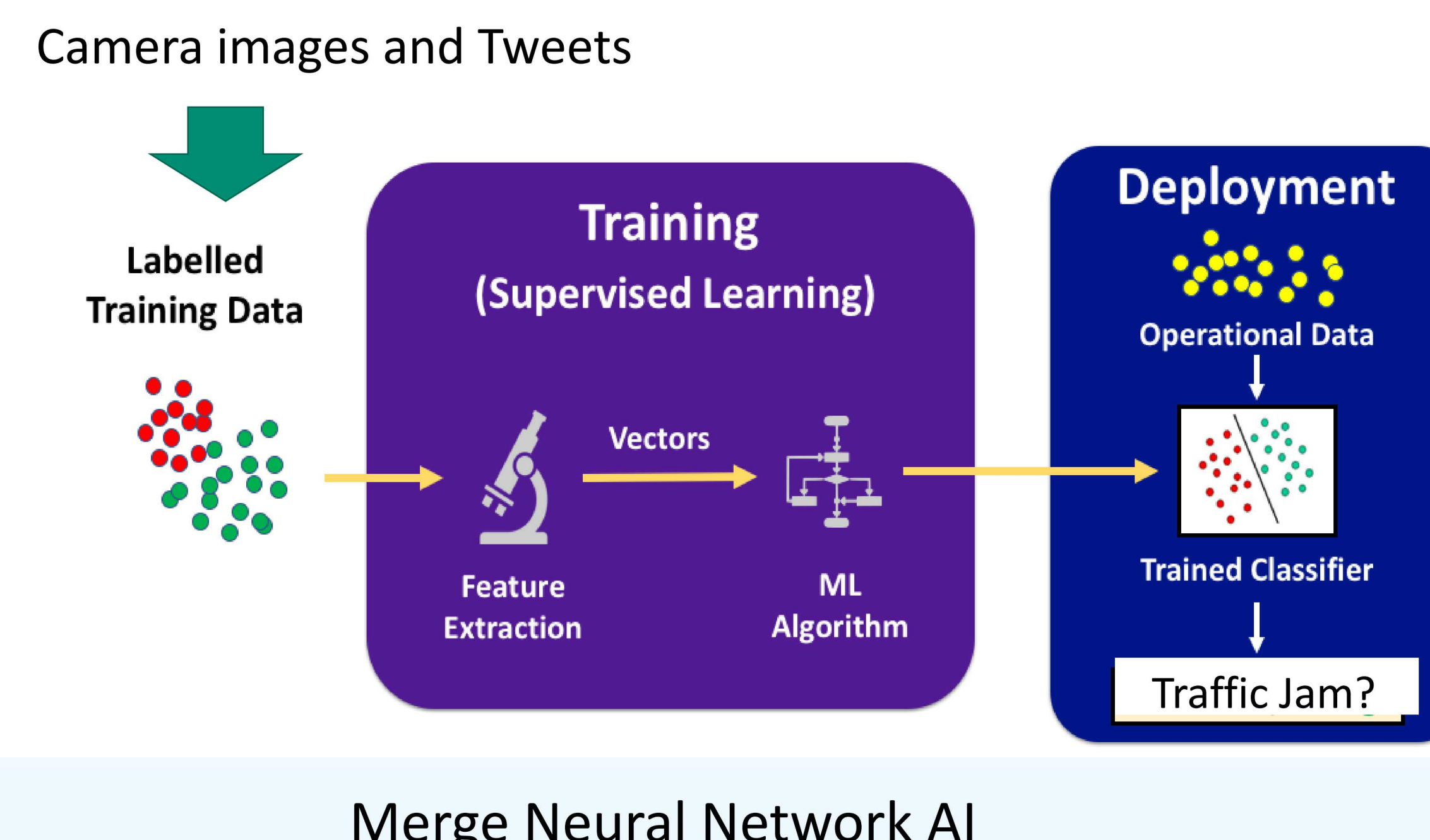


Challenges

- Scalability
 - Storage
 - Computing
 - Number of Data Sources
- Uncertainty quantification of information in decision making

Results

Exemplar Problem: Near-Real-Time Traffic Estimation Using Variety of Sources (without using GPS crowd sourcing (i.e. Google Maps))



Cat1: No Traffic Impact
 Cat2: Low Traffic Impact
 Cat3: High Traffic Impact

University of Illinois



Illinois Applied Research Institute



Sandia National Laboratories



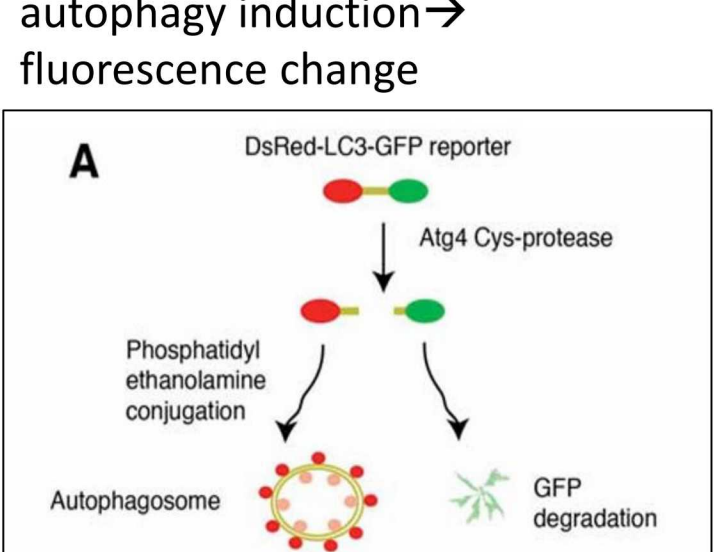


Introduction / Motivation

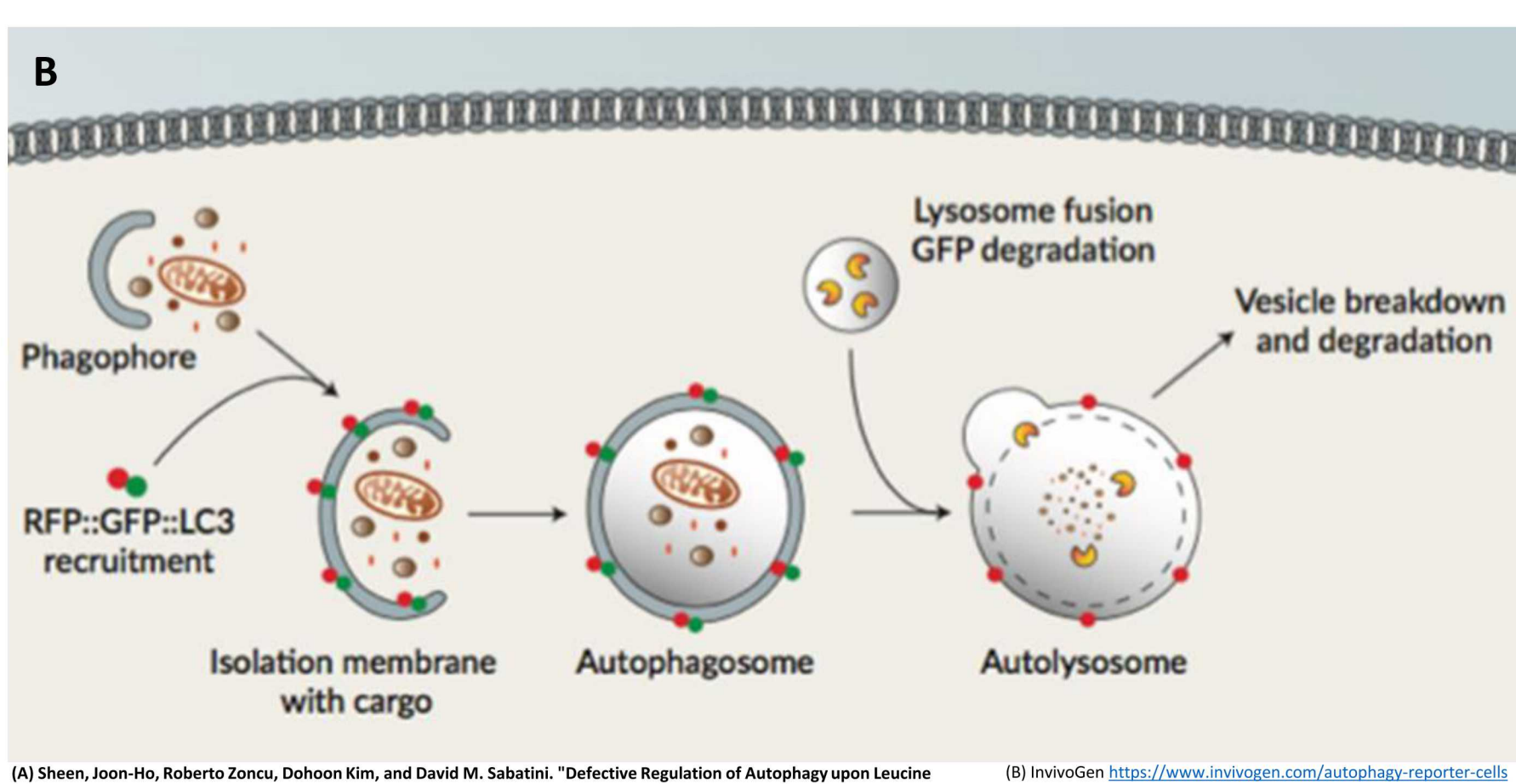
- Autophagy is a regulated process active in all human cells. It eliminates damaged organelles, removes toxic aggregated proteins, and acts as an autonomous defense against intracellular pathogens.
- Previous studies^[1] have displayed autophagy as having potential for therapeutic host-targeted control of mycobacterial infections through autolysosomal killing. This would limit the generation of antimicrobial peptides and potentially dangerous inflammation.
- Our goal is to demonstrate autophagy stimulation as a useful adjunct to antibiotic therapy in mycobacterial infections with the potential to limit drug resistant strains.

^[1] Bradfute, S. B., et al. (2013). "Autophagy as an immune effector against tuberculosis." *Current Opinion in Microbiology* 16(3): 355-365.

We have used an engineered HeLa DsRed-LC3-GFP autophagy reporter cell line to quantify drug-induced autophagy induction → fluorescence change



Increase in RFP with a concurrent decrease in GFP



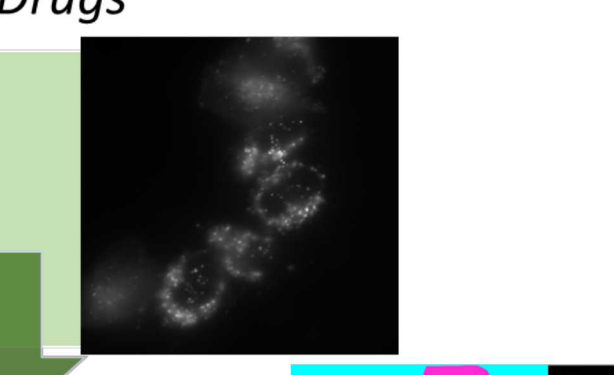
(A) Sheen, Joon-Ho, Roberto Zoncu, Dohoon Kim, and David M. Sabatini. "Defective Regulation of Autophagy upon Leucine Deprivation Reveals a Targetable Liability of Human Melanoma Cells In Vitro and In Vivo." *Cancer Cell* 19.5 (2011): 613-28. Web.

Challenges

Single-Cell Analysis of Autophagy Stimulating Drugs

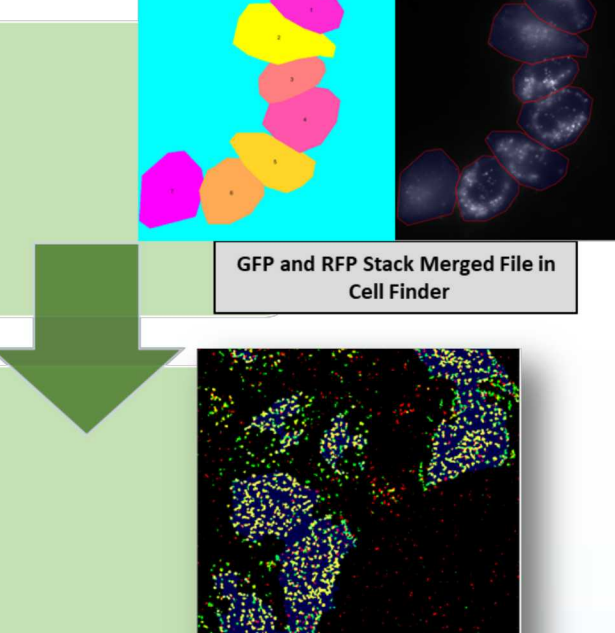
Step 1: Merge and Flatten Tiffs

In-house written software to merge and flatten the 14-stack tiffs to easily identify cells in the image.



Step 2: Segment Image to Identify Individual Cells

Utilize in-house written software, CellFinder, to identify the outline of individual cells in the images.



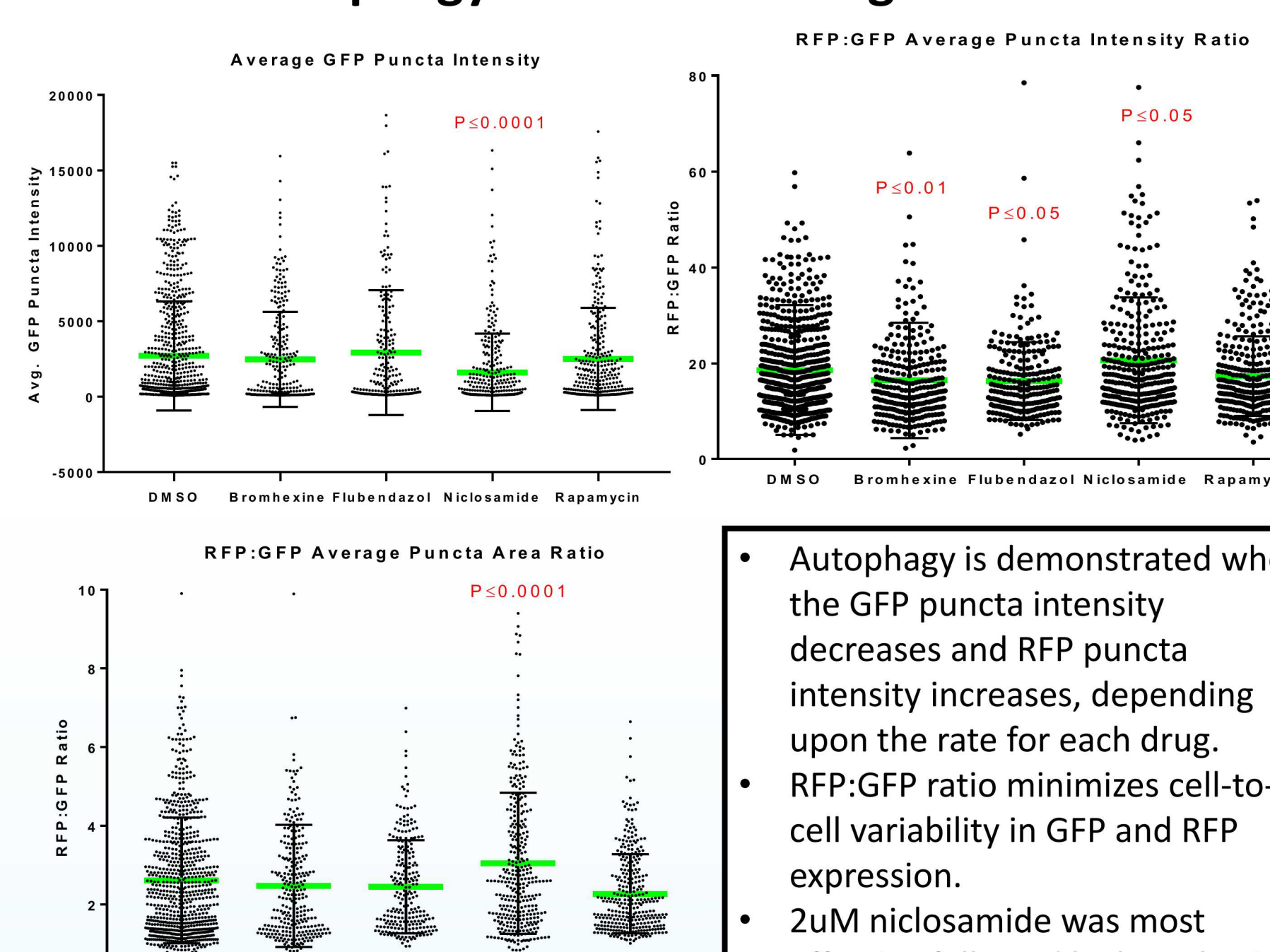
Step 3: Identify and Quantify Puncta in Both GFP and RFP Channels

In-house written software, BatchBiophagyCell, quantifies the number, intensity, and area of the puncta in each channel.

- Goal:** Identify number, area, and intensity of RFP and GFP puncta in individual cells
- Previous studies^[1] have measured autophagy induction by taking the average intensity over an entire image. The background intensity from multiple cells is a hindering variable producing less accuracy. 14 cell-based metrics were calculated and 3 selected to compare autophagy:
 - Average GFP intensity
 - RFP:GFP average puncta intensity ratio
 - RFP:GFP average puncta area ratio

^[1] Chauhan, S., et al. (2015) Pharmaceutical screen identifies novel target processes for activation of autophagy with a broad translational potential. *Nature Communications* 6, doi:10.1038/ncomms9620

Autophagy Induction in Single Cells



Single cell analysis was completed on a 14-slice confocal stack, where each condition has >250 cells. Statistical significance was determined by Mann-Whitney test followed by a Dunn's multiple comparison test to compare conditions to DMSO. Errors bars represent the SD from 3 independent experiments.

Results

Efficacy in a TB Surrogate

M. bovis infected RAW 264.7 Clearance			
Drug Treatment	Replication 1 (% Survival) MOI 3.75	Replication 2 (% Survival) MOI 0.75	Average % Survival
DMSO	100	92	96
Isoniazid	34.7	94.7	64.7
Niclosamide	240	70.7	155.35
Flubendazole	60	50.3	55.15
Bromhexine HCl	293	73.3	183.15
Rapamycin	20.7	46.7	33.7
Isoniazid + Niclosamide	6	49.3	27.65
Isoniazid + Bromhexine HCl	19.3	62.7	41
Isoniazid + Rapamycin	Contaminated	45.3	45.3
Isoniazid + Flubendazole	11.3	57.3	34.3

Fig. 2. RAW 264.7 infected with *M. bovis* to determine killing synergy based upon a multi-modal drug combination.

Percent survival of *M. bovis* in each replication. In replication 1, both niclosamide and bromhexine displayed >100% survival which could be attributed to *M. bovis* aggregates that form resulting in an uneven distribution in the CFU assay. In replication 1, Rapamycin was uncountable due to contamination.

- Each autophagy drug enhanced isoniazid killing.
- 2uM niclosamide in combination with 0.4ug/mL isoniazid was the most effective followed by flubendazole, bromhexine, and rapamycin combinations.

Future Work / Partnerships

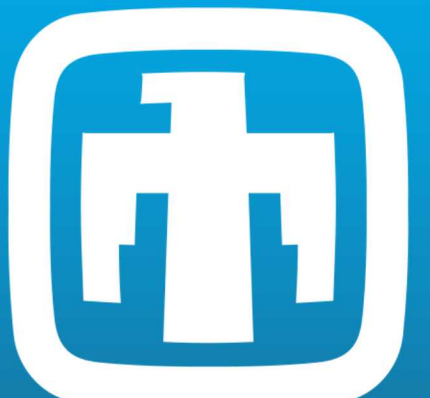
- Build on this model to characterize a set of new, proprietary antibiotics and autophagy stimulants. We will look at:
 - Autophagy stimulation efficacy
 - Antibiotic potency vs. isoniazid
 - Potential synergy of autophagy stimulants with isoniazid or the new antibiotics
- Identify potential drug binding sites and interactions within a human cell line.



Funding was provided by the NMSBA Program

TracerFIRE 8 Network

Michael Reeves, Purdue University; Israel Dennie, Bashiri Smith University of the Virgin Islands;



Introduction / Motivation

TracerFIRE is a Forensic and Incident Response Exercise program simulating a set of corporate-level cyber-attacks which produce realistic forensic artifacts.

For TracerFIRE to be effective, a realistic network infrastructure that can be infected with malware and allow for the collection of forensic artifacts is necessary. Due to hardware constraints and a portable platform prerequisite, the network needs to be virtualized. Additionally, the network needs to be customized for specific cyber attack killchains.

Approach

Construct a virtualized network, to host customized virtual machines and services for the TracerFIRE scenario. These are the technologies used to accomplish this:

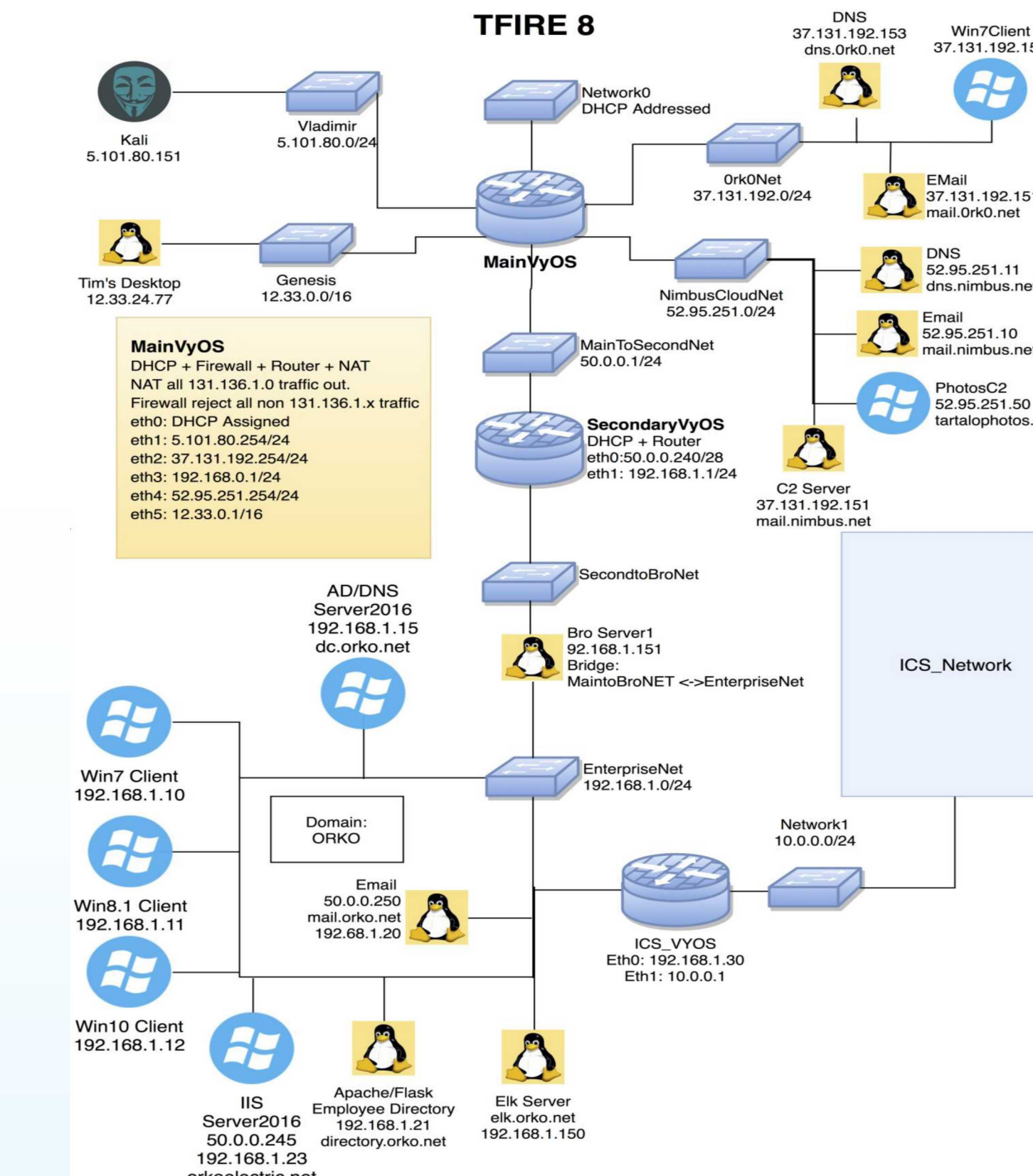
- VyOS – controls routing and manages firewalls within the network
- Xen Hypervisor – allows us to create and reproduce the virtual network across multiple hardware devices
- Bind9, Nginx, iRedMail – provides DNS, web and email services on corporate and attacker networks
- Apache/Flask - hosts the employee directory and syncs with AD using LDAP
- Ubuntu/Debian OS – hosts opensource web services
- Windows Server 2016 – hosts AD/DC, DNS, and IIS
- Bro Service – logs network traffic for analysis
- Filebeat and ELK Stack - used to forward, view, and search network logs
- Orchestration framework - emulates a realistic ICS network

Challenges

- Manipulation of Virtual machines and Networks on the Xen Hypervisor
- Windows network administration and enterprise management
- Using the DNS within the confines of the TracerFIRE scenario
- Successful execution and simulation of attack chains on the network.

Results

- A virtualized network that can be redeployed on multiple Xen instances
- A network infrastructure that supports the requirement of the TracerFIRE scenarios
- The network allows malware infection within a simulated corporate network



Future Work / Partnerships



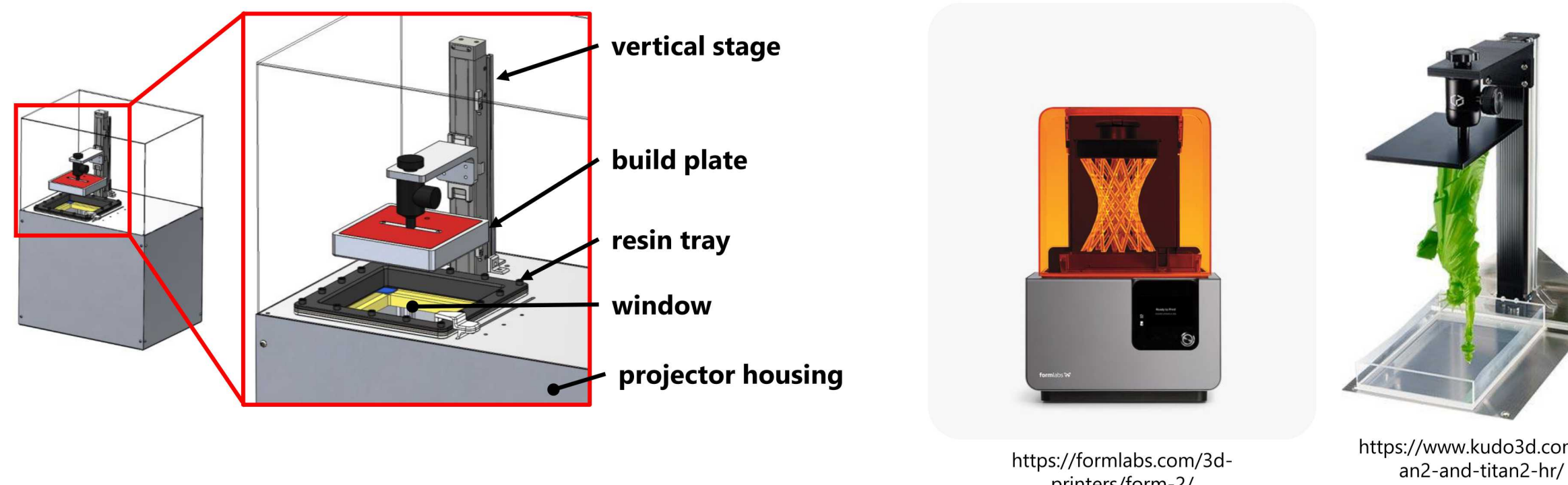
Mechanical Challenges of 3D Printing Ceramics Using D.L.P.

Matthew A. Roach, David Keicher, Erin Maines, Benjamin Wall, Christopher Wall, Judith Lavin, Shaun Whetten, Lindsey Evans



Introduction / Motivation

Digital light processing (DLP) 3D printing can be used for manufacturing complex structures using a variety of materials, which would be nearly impossible using traditional manufacturing methods. Recent work at Sandia National Laboratories uses DLP technology for additive manufacturing of complex alumina structures, using photocurable resins loaded with micron or submicron alumina particles. These resins are printed using a DLP 3D printer to produce a "green part." The work presented here will discuss the mechanical challenges associated with printing alumina using commercially available DLP and stereolithography 3D printers, including the design of a custom DLP 3D printer to address identified mechanical challenges, thereby leading to improved print versatility and quality.

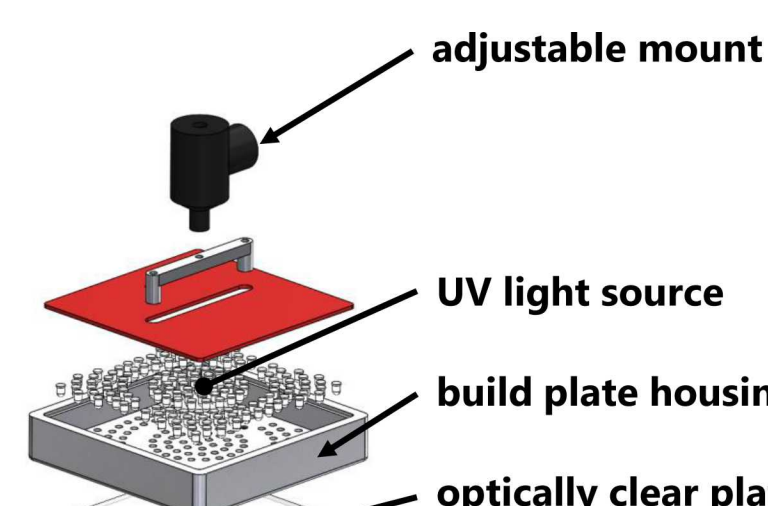


Custom Printer

UV Backlit Build Plate

The UV backlit build plate is intended to:

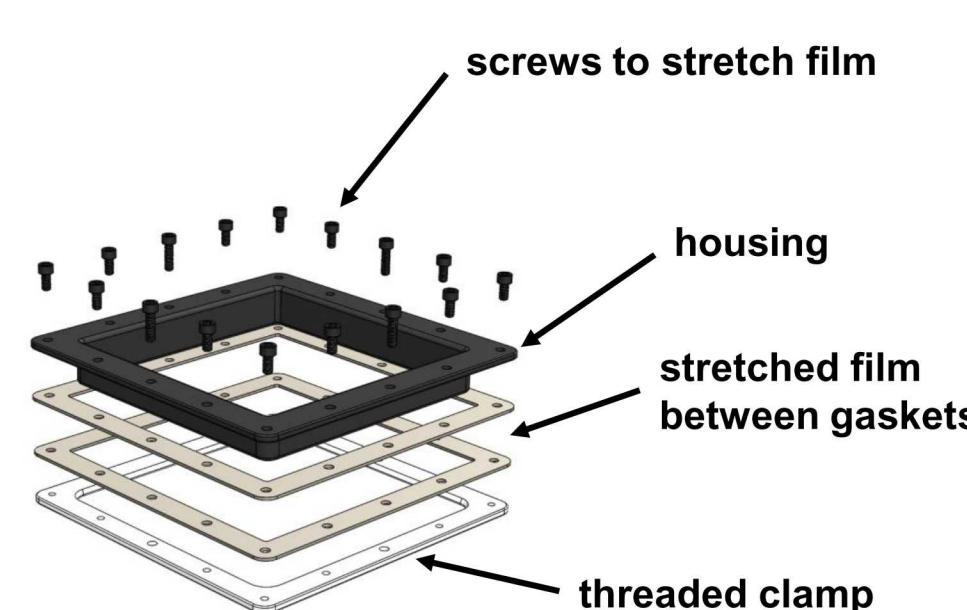
- Ensure strong build adhesion
- Provide a level surface between resin tray and build surface



Stretched Film Resin Tray

The stretched film resin tray is intended to:

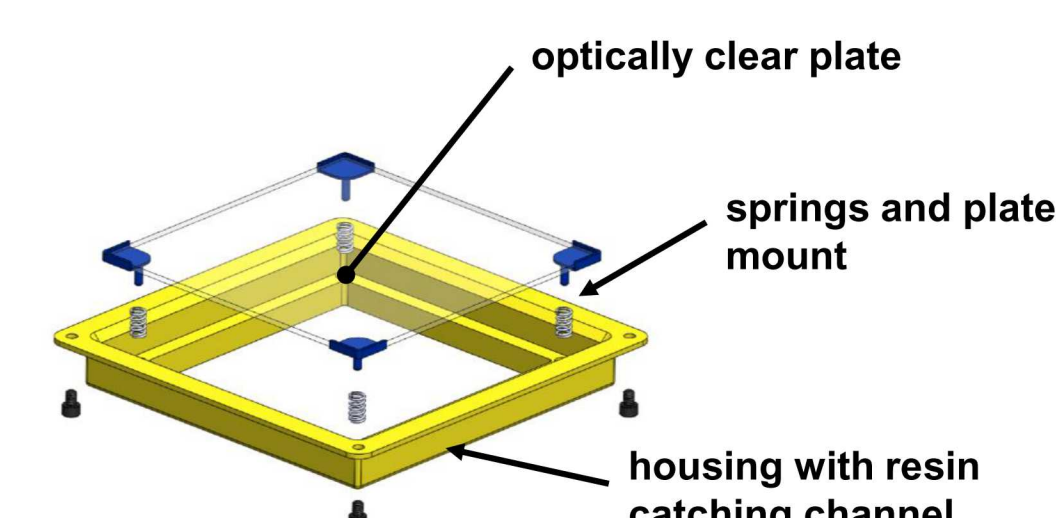
- Allow builds to slowly release from resin tray
- Reduce force on build due to separation
- Provide an optically clear, durable, surface to build from



Glass Support Plate

The glass support plate is intended to:

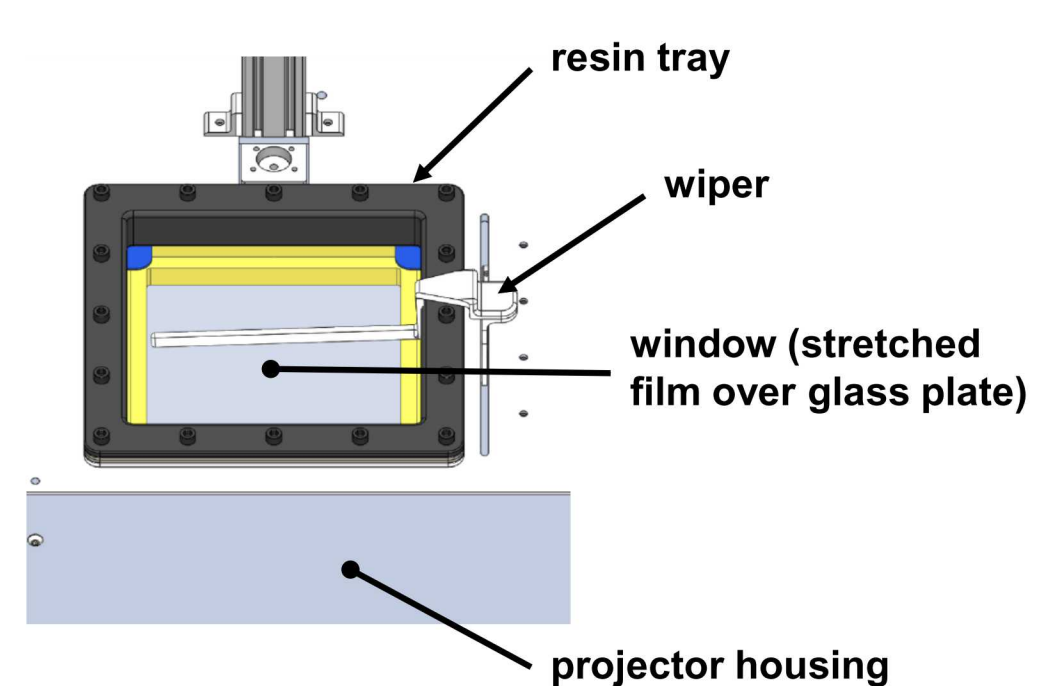
- Provide a level surface for the stretched film to come in contact with
- Provide a level surface for the build plate to allow for uniform layer thickness
- Prevent damage to print surfaces and printer



Wiper Bar

The wiper bar is intended to:

- Remove over cured materials from active print area
- Agitate material to prevent particle settling

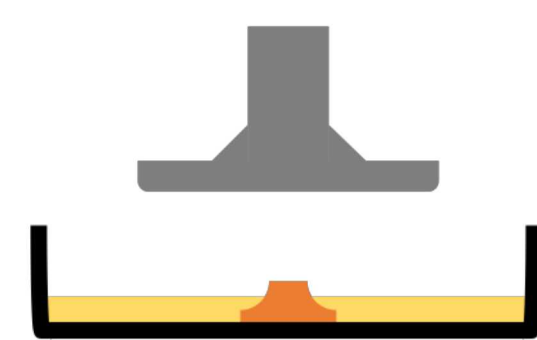


Challenges

Dropping

Dropping occurs when the initial layers of the build are not strongly adhered to the build plate.

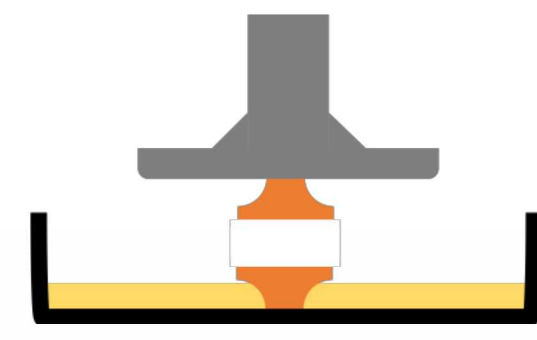
Solution: UV-Backlit build plate



Splitting

Splitting occurs when the force of separation on the build is too great, resulting in a build fracture.

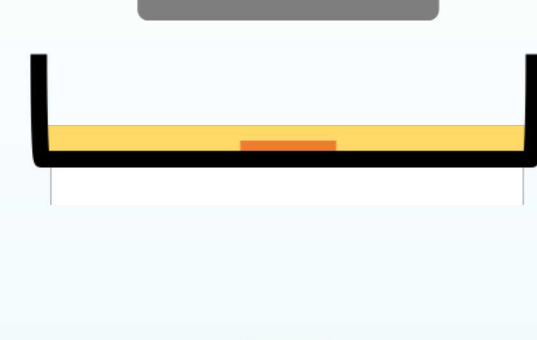
Solution: Stretched film resin tray



Sticking

Sticking occurs when the build plate does not have adequate contact with the resin tray.

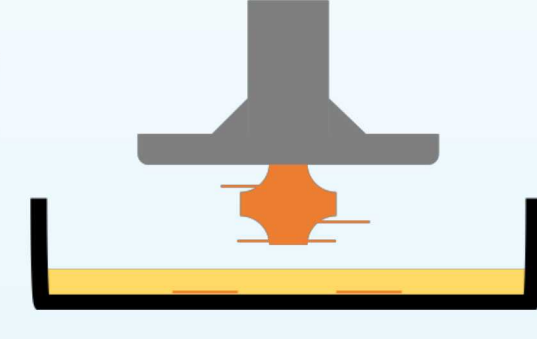
Solution: Glass support plate



Flaking

Flaking occurs due to the over-curing of resin. This over-curing occurs frequently in advanced materials.

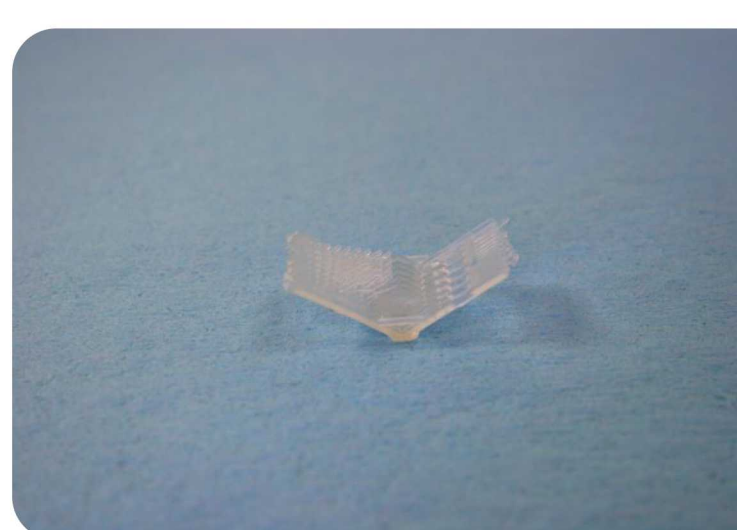
Solution: Wiper bar



Results

Standard Resin

- Genesis (By Tethlon 3D)
- 25 μm layer resolution
- Scratched copper build plate
- Basic functionality proven



Silica Loaded

- Porcelite (By Tethlon 3D)
- 25 μm layer resolution
- UV backlit build plate
- Ability to build using loaded resins proven



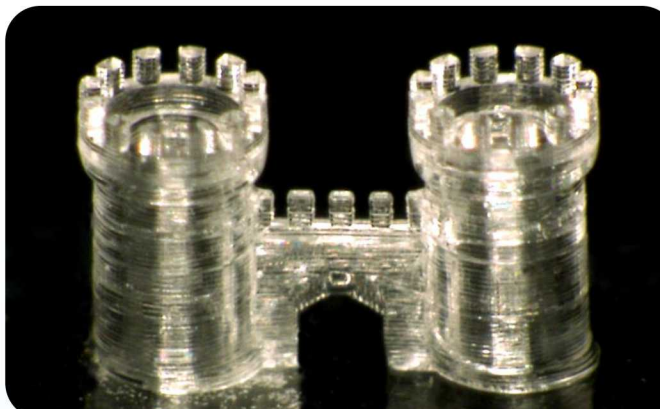
Alumina Loaded

- Alumina loaded resin (Custom material)
- 25 μm layer resolution
- UV backlit build plate
- Proven some functionality building with alumina



Future Work

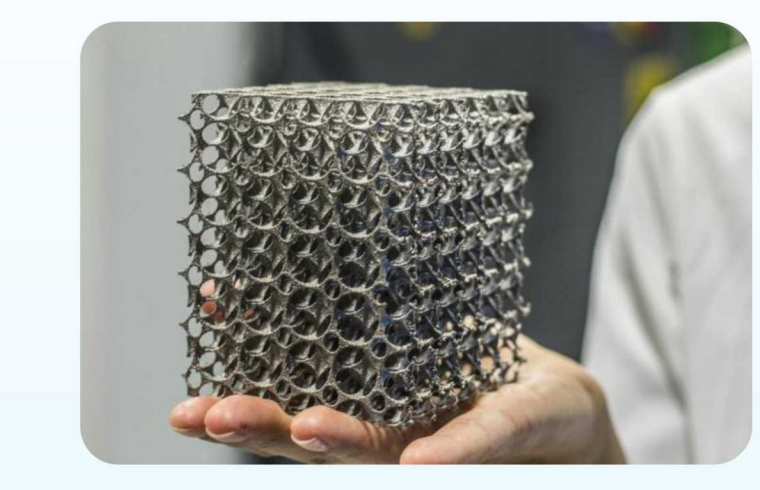
- Finalize prototype design and further iterations
- Custom control program
- Larger UV-backlit build plate, for larger production of printed parts without creating longer print times (when using DLP technology)
- Heated build chamber, for finer resolution by exploiting changes in resin curing at different temperatures (Hot Lithography).
- Alternative high-performance materials such as glass and metals



<https://phys.org/news/2017-04-d-glass.html>



<http://tethlon3d.com/product/porcelain-ceramic-resin/>



<http://engatech.com/metal-3d-printing/>



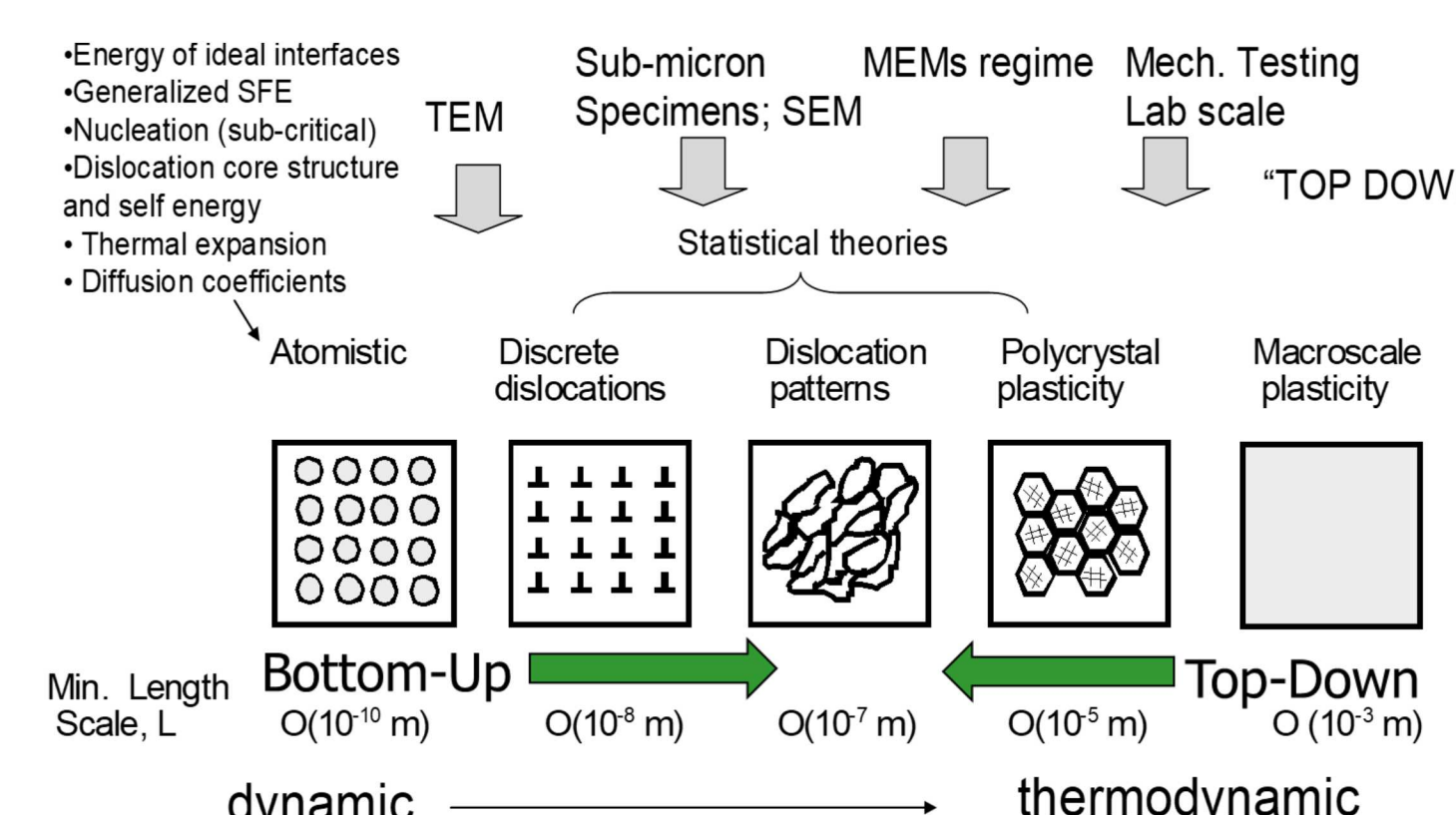
Introduction / Motivation

Computational materials models exist at multiple scales with different parameterizations.

- How do models/scales connect?
- Which data are relevant to a prediction?

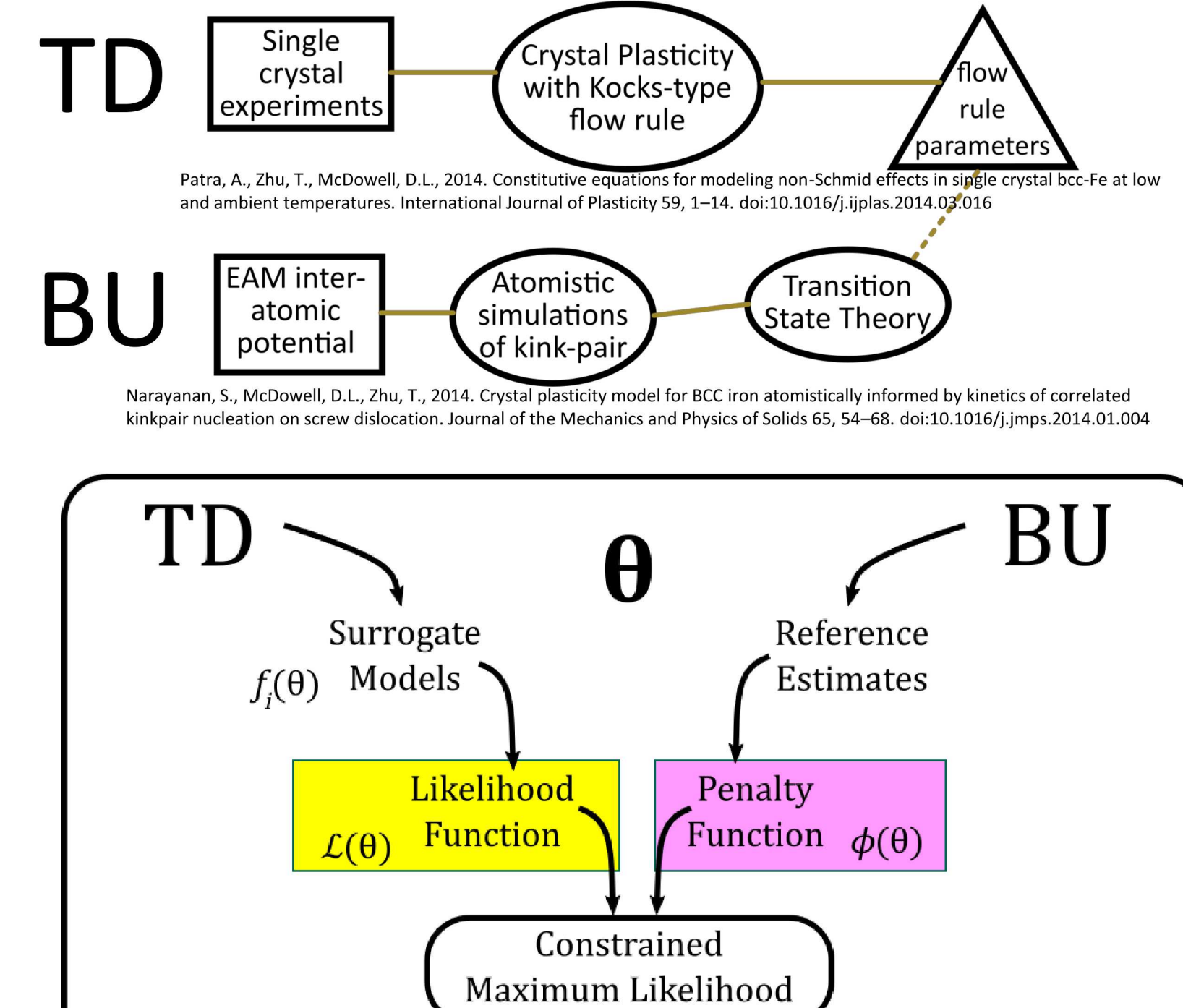
GOAL: Advance data collection strategies to:

- Perform Top-Down/Bottom-Up reconciliation of parameters
- Test empirical support of a connection between models



Approach

Reconciled Top-down and Bottom-up Hierarchical Multiscale Calibration of bcc Fe Crystal Plasticity



- Calibration parameters: θ
- To be TD and BU, models must meet in the middle → value(s) for θ , $\hat{\theta}_{TDBU}$

- Where is the middle? Use likelihood-based methods to reconcile
- Constrained Likelihood: Maximum → middle

$$\text{Top-Down:}$$

$$\text{Likelihood}(\theta) \cong \exp \left(-\frac{1}{2} \sum_{i=1}^{N_{\text{data}}} \frac{(f_i(\theta) - Y^E(x_i))^2}{\sigma_{\text{exp},i}^2} \right)$$

$$\text{Penalty}(\theta)_j = \exp \left(-\frac{1}{2} \frac{(\theta_j - \hat{\theta}_{BU,j}^{\text{ref}})^2}{\sigma_p^2} \right)$$

$$\text{Bottom-Up}$$

$$\text{Constrained Likelihood}(\theta) = \text{Likelihood}(\theta) \prod_{j=1}^{n_p} \text{Penalty}(\theta)_j$$

$$\text{Reconciliation} \rightarrow \max(CLF(\theta)) \Rightarrow \hat{\theta}_{TDBU}$$

Challenges

Need to evaluate the difference between $\hat{\theta}_{TDBU}$ and $\hat{\theta}_{TD}$. What is the cost and uncertainty associated with adding bottom-up information?

We formulate a connection cost "u" between TD and BU routes:

$$CLF(\theta | \text{Uncertainty}) = CLF(\theta)^u, u \in (0, 1]$$

$u = 0$: infinite connection cost, no agreement at all between TD and BU data

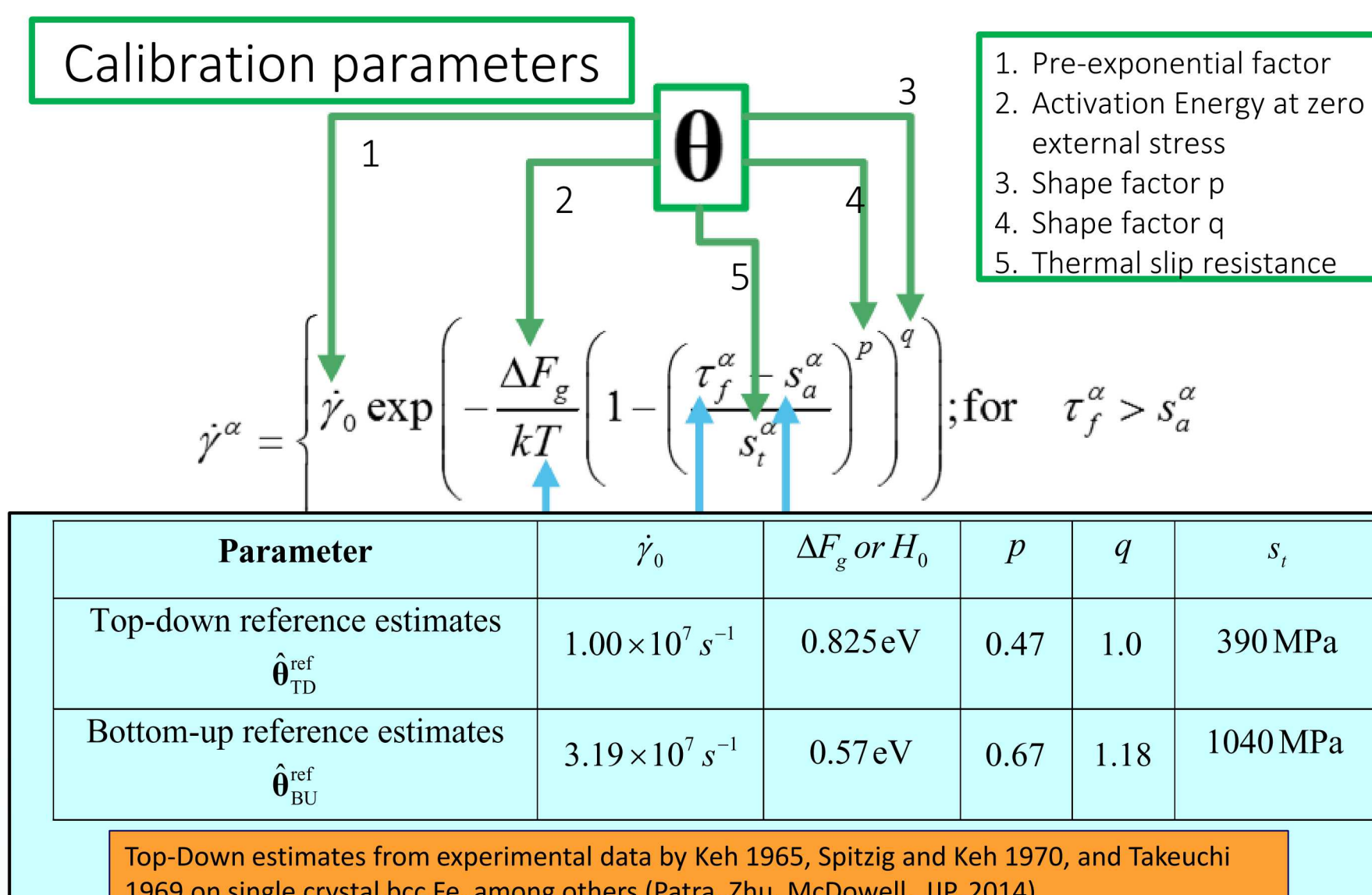
$u = 1$: no connection cost; no disagreement between TD and BU data

$$u = \frac{1}{\max \{ \text{SSE} + \text{Penalty}(\hat{\theta}_{TDBU}), 1 \}} = \frac{1}{\max \{ -2 \ln (CLF(\theta | \theta = \hat{\theta}_{TDBU})), 1 \}}$$

$$PDF(\theta) = \frac{CLF(\theta)^u \text{ Prior}(\theta)}{\text{Normalizing Const.}}$$

$$\sigma_{\theta}^2 = \int_{\theta-\text{space}} PDF(\theta) \sum_{j=1}^{n_p} (\theta_j - E[\theta_j])^2 d\theta$$

Results



Parameter	$\dot{\gamma}_0$	ΔF_g or H_0	p	q	s_t
Top-down reference estimates $\hat{\theta}_{TD}^{\text{ref}}$	$1.00 \times 10^7 \text{ s}^{-1}$	0.825 eV	0.47	1.0	390 MPa
Bottom-up reference estimates $\hat{\theta}_{BU}^{\text{ref}}$	$3.19 \times 10^7 \text{ s}^{-1}$	0.57 eV	0.67	1.18	1040 MPa

Top-Down estimates from experimental data by Keh 1965, Spitzig and Keh 1970, and Takeuchi 1969 on single crystal bcc Fe, among others (Patra, Zhu, McDowell, IJP, 2014)

$\hat{\theta}_{BU}^{\text{ref}}$	$\dot{\gamma}_0$	ΔF_g or H_0	p	q	s_t
Simulated	$3.19 \times 10^7 \text{ s}^{-1}$	0.57 eV	0.67	1.18	1040 MPa
"cooperative"	$1.58 \times 10^7 \text{ s}^{-1}$	0.75 eV	0.48	1.3	540 MPa
"spurious"	$5.00 \times 10^5 \text{ s}^{-1}$	0.95 eV	0.8	1.5	1100 MPa

BU estimate $\hat{\theta}_{BU}^{\text{ref}}$	Calib.	SSE	SSE + Penalty	u	σ_{θ}^2
Simulated	TD	37.7	161.7	5.98×10^{-2}	0.296
	TDBU	83.1	102.3	1.17×10^{-2}	0.317
"cooperative"	TD	37.7	81.0	5.98×10^{-2}	0.296
	TDBU	56.1	57.5	4.34×10^{-2}	0.249
"spurious"	TD	37.7	262.6	5.98×10^{-2}	0.296
	TDBU	78.0	224.4	5.69×10^{-3}	0.340

Results summary

- u decreases with more data (implying more cost)
- After including the atomistic simulations, the σ_{θ}^2 value increased versus TD-only except for cooperative case
- Interpretation: only cooperative connection is helpful
- Diagnosis: many lines of inquiry to follow
- Parameter set may be a limitation, Peierls stress may be Temp dependent Mori, H., Temperature and Stress Dependence of Mobility of Screw Dislocation in BCC Iron, Solid State Phenomena, vol. 258, pp. 17–20, 2017.
- Choice of interatomic potential / constitutive laws may alter outcome Lim, H., Hale, L.M., Zimmerman, J.A., Battaile, C.C., and Weinberger, C.R., A multiscale model of dislocation plasticity in α -Fe: Incorporating temperature, strain rate and non-Schmid effects, International Journal of Plasticity, vol. 73, pp. 100–118, 2015

Collaborative efforts

Tallman, A.E., Swiler, L.P., Wang, Y., McDowell, D.L., 2017. Reconciled Top-down and Bottom-up Hierarchical Multiscale Calibration of bcc Fe Crystal Plasticity. JMC 15. <https://doi.org/10.1615/IntMultCompEng.2017021859>

Special Issue Editors Yan Wang of Georgia Tech and Laura Swiler of Sandia: ASCE-ASME Journal of Risk and Uncertainty in Engineering Systems, Part B: Mechanical Engineering. Special Issue on Uncertainty Quantification in Multiscale System Design and Simulation. ASME J. Risk Uncertainty Part B. 2017; 4(1):010301-010301-2. doi: 10.1115/1.4037447.

Laura Swiler served on Aaron Tallman's thesis committee (Ph.D. defense in July 2018). Book chapter and papers coming.

Note: The figures have been reproduced with permission from (Tallman, 2017) and Tallman's thesis: "Hierarchical Multiscale Materials Modeling: Calibration, Uncertainty Quantification, and Decision Support," 2018.